ATL-LARG-PUB-2007-012
08 November 2007

Calibration of the ATLAS electromagnetic calorimeter using calibration hits

D. Banfi, L. Carminati, L. Mandelli
Dipartimento di Fisica dell' Universita' degli Studi e Sezione INFN di Milano

July 11, 2007

Abstract

In the present note a method to determine the electron energy from the energies measured in an electron cluster is discussed. The method is based on a detailed Monte-Carlo simulation (labeled *Calibration Hits*) of electrons in the ATLAS detector in which also the energies deposited in the passive and dead materials are recorded. It allows also to compute the different contributions (energy deposited in front, in and behind the Accordion) to the total electron energy. To better understand the various contributions to the energy reconstruction three rounds of simulations have been performed: electrons hitting the middle cell centre, electrons spread uniformly over a cell in absence of magnetic field and electrons spread uniformly over a cell in presence of magnetic field. The method is applied to the Barrel calorimeter and to electrons. Its extension to the End Caps and to photons does not pose problems. In the operative ATLAS conditions an energy resolution sampling term varying from 9.9% at η=0.3 and 16.8% at η=1.2 is obtained. The linearity varies between 0.1% and 0.4% in the energy interval 10-100GeV over the same η range.

Contents

1 Introduction

In this note a method to compute the electron energy from the energy deposited in the active layers of the calorimeter and the presampler is described. What is proposed is a development of ideas introduced in ([1, 2, 3]) to analyze test beam data. Special simulations, labeled *Calibration Hits* are used. In these simulations the energy deposited by a particle in all the materials of the detector and not only in the active ones like in the standard simulation, is recorded. Using these simulations the energy depositions in inactive materials is correlated to measurable quantities.

The aim of the method is to provide a modular way to calibrate electrons (and photons in the future) by decoupling the corrections for the energy lost in front, in and besides the calorimeter. For example the energy lost in the material in front of the calorimeter is computed from the energy deposited in the presampler. This approach will allow to study differences/similarities between electrons and photons and provide a flexible way of calibrating egamma objects which might be useful when the decoupling of the corrections is required.

To disentangle different effects contributing to the energy reconstruction, three different rounds of simulation have been used at various fixed η positions and energies.

- electrons hitting the centre of a middle cell compartment. No magnetic field in the tracker region. These are the simplest possible conditions.
- electrons spread uniformly over the middle cell compartment. No magnetic field. These simulations are used to study the effects introduced by the Accordion granularity.
- electrons spread uniformly over the middle cell compartment in presence of the magnetic field. These simulations reproduce the real conditions in ATLAS.

In section 2 the ATLAS electromagnetic calorimeter is briefly discussed. The method is described in section 3 while its application in the three cases reported above is described in sections 4,5,6.

2 The ATLAS Liquid Argon Electromagnetic Calorimeter

In the present section a few details of the ATLAS electromagnetic calorimeter relevant for the discussion of the calibration method are briefly reviewed: further details can be found in ([4]). The ATLAS electromagnetic calorimeter is

a lead/liquid Argon sampling calorimeter with Accordion shaped electrodes and absorbers interleaved as sketched in figure (1).

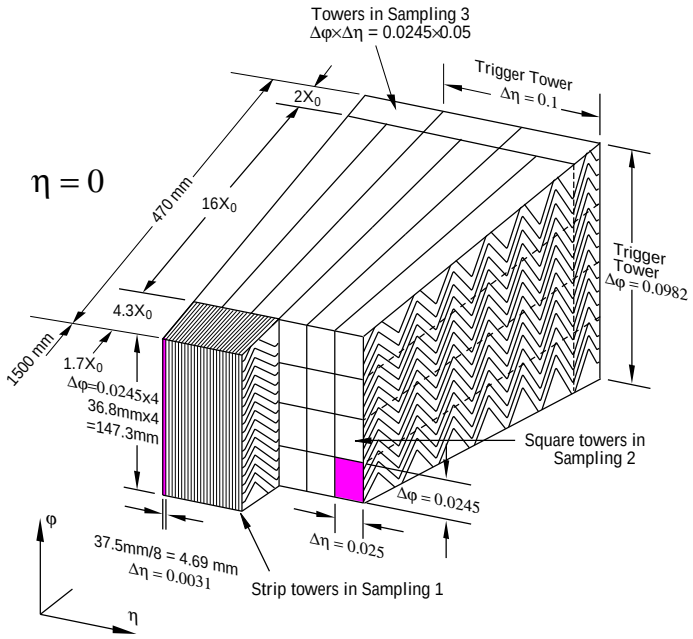

Figure 1: Segmentation of the EM barrel calorimeter

The absorbers are made of lead glued between thin stainless steel sheets with a total thickness of 2.2 mm. In the barrel, in order to maintain an approximately constant number of radiation lenghts over the entire barrel pseudorapidity range, the lead thickness decreases from 1.5 to 1.1 mm at $\eta = 0.8$. The electrodes are flexible three layer Cu-Polymide printed circuit boards. The two outer layers are connected to HV while the inner layer collects the signal by capacitive coupling.

The calorimeter is divided in two half-barrel cylinder covering the pseudorapidity range $|\eta| \leq 1.475$ housed in a single cryostat (together with the solenoid superconducting coil placed in front of the calorimeter which provides the inner magnetic field) and two end-cap detectors (covering the $1.375 \leq |\eta| \leq 3.2$ range) housed in two separate end-cap cryostats.

The calorimeter is segmented in ϕ, η and depth. The readout granularity in ϕ is obtained by summing signals of a certain number of gaps. The separation in longitudinal compartments and in η cells is made by etching on the copper surface of the electrodes. Except for the edge zones such as the transition region at $|\eta| \simeq 1.5$ between barrel and end-caps, the segmentation of the calorimeter has three compartments in depth while both η and ϕ granularity depends on the compartment:

1. The first sampling (*strips*) ends at about 5 X_0 including $\simeq 1.5$ X_0 (depending on η) of dead upstream material in the ATLAS configuration. It has a fine η - segmentation (0.003 equivalent to 5 mm at $\eta = 0$) while it is more coarse in ϕ (0.1). It is optimized for γ/π^0 separation and allows a good photons direction reconstruction.

2. The second sampling (*middle*) contains most of the shower energy and ends after about 22 X_0 (depending on η). Its granularity is $\Delta\eta$ x $\Delta\phi = 0.025$ x 0.025.

3. The third sampling (*back*) has twice the granularity in η of the middle layer (0.05) while the same granularity in ϕ.

The total thickness (in X_0) as a function of η of the electromagnetic calorimeter is reported in figure2.

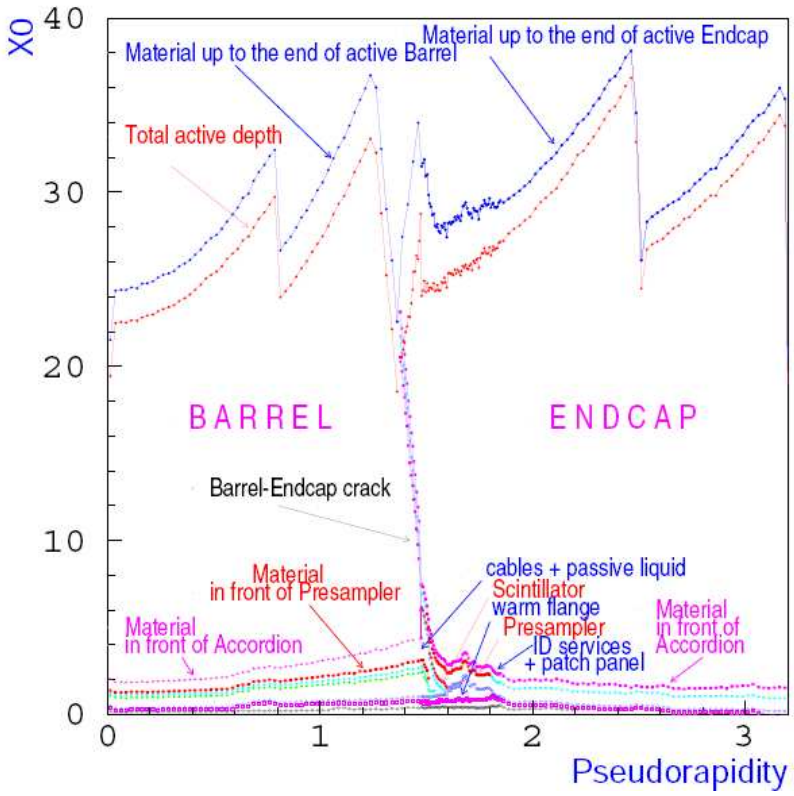

Figure 2: Total thickness (in X_0) as a function of η of the electromagnetic calorimeter

In the $|\eta| \leq 1.8$ range a thin presampler detector is placed in front of the calorimeter to have additional information on the energy losses in the dead material in front of the calorimeter.

3 Description of the method

As stated at the beginning the use of a special MC simulation of the ATLAS setup based on GEANT 4.7 in ATHENA 10.0.1 is made. In these simulations the ionization currents, their digitization and the signal reconstruction are not activated. All hits are stored in different containers depending on the material: the materials inside the ATLAS detector simulation are classified into tree different classes:

- active: all active layers in any subdetector volumes. For example the LAr between the electrodes of the Accordion
- inactive: all inactive layers in any subdetector volumes. For example the absorbers of the Accordion
- dead: for example the solenoid, the cryostat, etc.

A self made code including a clusterization algorithm is used. In the present study clusters of $\eta \times \phi = 3 \times 5$ are reconstructed around the most energetic cell. The following energy depositions are computed directly from the Monte-Carlo.

- E_{front} : total energy deposited in front of the preshower, including the tracker, the cryostat and the solenoid.
- E_{ps} : energy deposited in the preshower, divided in *active*/*inactive*
- E_{psstr} : energy deposited in the inactive material between preshower and first Accordion compartment (strips)
- E_i : energy deposited in the *ith* (i=1,3) sample of EM calorimeter, divided in *active*/*inactive* and *in/out* of cluster
- E_{leak} : total energy deposited behind the third sample of the EM calorimeter (cables, LAr, cryostat, hadronic calorimeter, etc).

The flow of the proposed method with reference to the formula (1) is the following:

1. Reconstruction of the energy deposited in the Accordion inside the cluster.
2. Estimation of the energy deposited in the Accordion outside the cluster.
3. Reconstruction of the energy leaked beyond the electromagnetic calorimeter.

4. Estimation of the energy in the materials in front of the calorimeter as a function of the energy deposited in the presampler: as it will be shown in the following this parameterization depends on the energy of the incoming particle but could be successfully parametrized as a function of the energy deposited in the Accordion.

In more detail the electron energy will be reconstructed with the following formula:

$$\begin{aligned} E_e &= a(E_{tot}^{Acc},\eta) + b(E_{tot}^{Acc},\eta)\cdot E_{ps}^{clLAr} \\ &+ \frac{1}{s_{cl}^{Acc}(X,\eta)\cdot f_{out}(X,\eta)}\cdot\Big(\sum_{i=1,3} E_i^{clLAr}\Big)\cdot(1+f_{leak}(X,\eta))\cdot(F(\eta,\phi)) \quad (1) \end{aligned}$$

Where:

- E_e is the electron energy
- $a(E_{tot}^{Acc},\eta)$ and $b(E_{tot}^{Acc},\eta)$ are parameters to be determined as a function of the energy deposited in the accordion (E_{tot}^{Acc}) and η and labeled *offset* and *slope*. Unlike the methods used in [1, 3] where the energy deposited in the materials in front of the presampler and the energy deposited between the presampler and the strips are computed by two separate terms, in this note a single term including both contributions is adopted. A single term, while keeping the same performance in terms of resolution and linearity decreases the number of required parameters .
- E_{ps}^{clLAr} is the energy deposited in the active material of the preshower in the cluster
- X is the the longitudinal barycenter of the shower (called *Shower Depth* in the text) defi ned by (2):

$$X = \frac{\sum_{i=0}^{3} E_i^{clLAr} X_i}{\sum_{i=0}^{3} E_i^{clLAr}} \quad (2)$$

  where: E_i^{clLAr} are the energies deposited in the active medium of the preshower and the three compartments of the calorimeter (strip, middle, back), and X_i is the depth, expressed in radiation length, of the longitudinal centre of each compartment computed from the interaction point (centre of ATLAS in this simulation). X_i are functions of η (Fig(3)).
- $s_{cl}^{Acc}(X,\eta)$ is the Accordion sampling fraction in the cluster. It will be parametrized as a function of X and η.

- $f_{out}(X, \eta, E_e)$ is the correction for the energy deposited in the calorimeter outside the cluster. In absence of magnetic field f_{out} is fairly independent from the electron energy when expressed as a function of X. In this case an inclusive correction labelled *Total Accordion Correction Factor* is applied. It will be parametrized as a function of X and η.

- $f_{leak}(X, \eta)$ is the longitudinal leakage correction. It will be parametrized as a function of η and X.

- $F(\eta, \phi)$ is the energy correction depending from the impact point inside a cell (*energy modulation*).

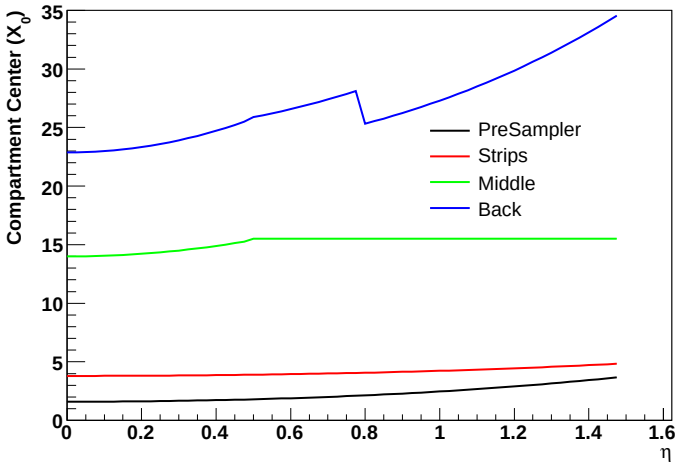

Figure 3: Compartment center (in X_0) as a function of η of the electromagnetic calorimeter

All electrons are simulated from the ATLAS centre. Few samples of events simulated with a vertex spread show that the vertex spread influences only the energy modulation inside a cell and not the other terms of the reconstruction algorithm.

4 Electrons hitting the cell centre

To study, understand and explain the proposed calibration method the simplest conditions are used at the beginning: electrons hitting the centre of a cell (middle compartment).

To determine the calibration constants as a function of η and the electron energy 11 points in η (spanning from η=0.1 to η=1.2 with 0.1 steps) and 11 values of energy (5, 10, 15, 20, 30, 40, 50, 60, 80, 100, 200 GeV) are simulated. The statistics of each sample is 10k.

4.1 Energy Reconstruction in the Accordion

The energy deposited by the electron shower in the Accordion is first reconstructed. Figure (4) shows the Accordion sampling fraction as defined in equation (3) for four different η values.

$$s_{tot}^{Acc} = \frac{E_{LAr}^{Acc}}{E_{LAr}^{Acc} + E_{Abs}^{Acc}} \tag{3}$$

where: E_{LAr}^{Acc} is the total energy deposited in the active medium (LAr) of the Accordion , and E_{Abs}^{Acc} is the total energy deposited in the Accordion inactive materials.

In figure (5) the cluster sampling fraction defined in equation (6) is shown for the same η values.

$$s_{cl}^{Acc} = \frac{E_{clLAr}^{Acc}}{E_{clLAr}^{Acc} + E_{clAbs}^{Acc}} \tag{4}$$

where: E_{clLAr}^{Acc} is the energy deposited in the Accordion active medium (LAr) inside the cluster, E_{clAbs}^{Acc} is the energy deposited in the Accordion inactive materials inside the cluster.

The cluster sampling fraction s_{cl}^{Acc} shows the same behavior as the Accordion sampling fraction s_{tot}^{Acc}, but its value is about 1 % higher. This is due to the fact that in an electron shower the fraction of very low energy photons and electrons increases with the radial distance from the shower center. These low energy particles are more easily absorbed in the lead.

The cluster sampling fraction, when integrated over X, is energy dependent as is shown in figure (6). However this dependence is almost completely absorbed in the dependence from the shower depth.

The fraction of energy deposited outside the cluster as defined in equation (5):

$$E_{out}^{cl} = \frac{E_{out}^{clLAr}}{E_{Abs}^{Acc} + E_{LAr}^{Acc}} = 1 - f_{out} \tag{5}$$

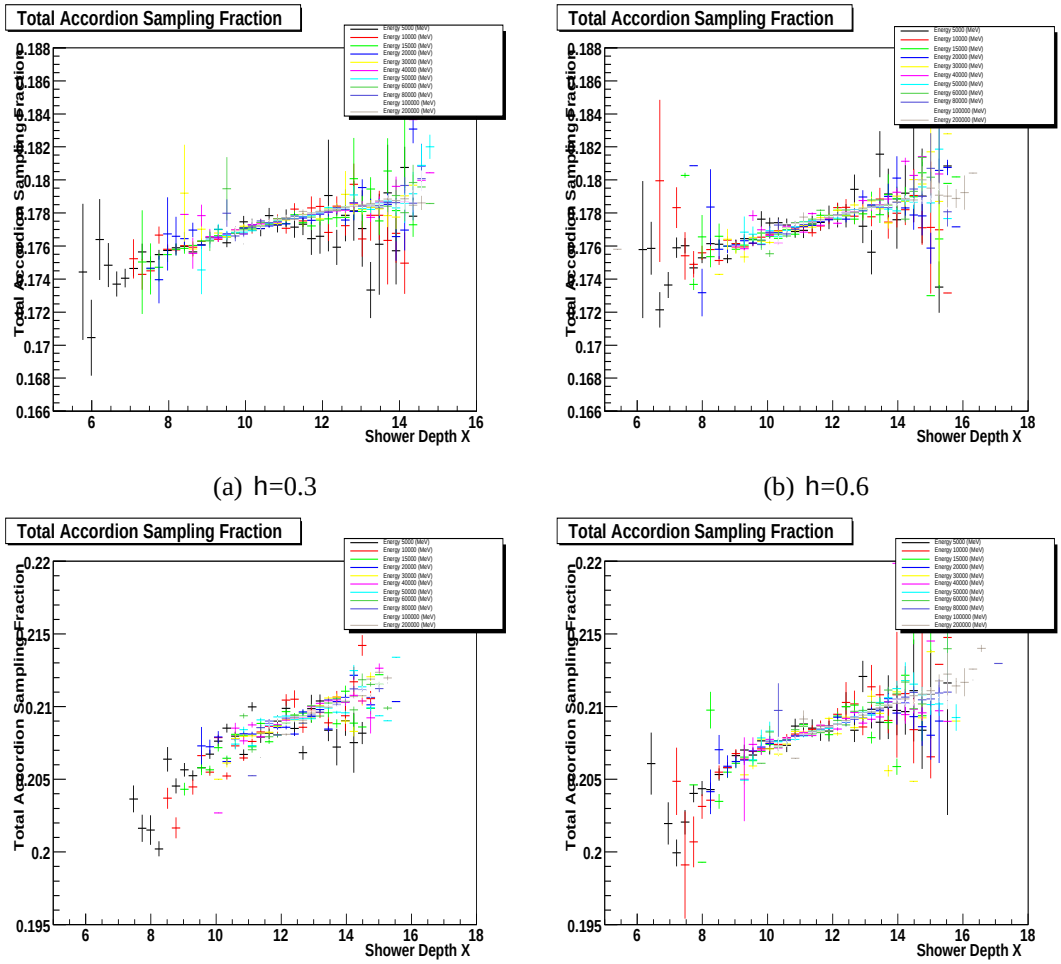

(a) h=0.3 (b) h=0.6

(c) h=0.9 (d) h=1.2

Figure 4: Accordion Sampling Fraction as a function of the shower depth X for various electron energies and h values.

is shown in figure (7).

Once considered as a function of the shower depth also this quantity is fairly energy independent. A non negligible energy dependence is visible at large h for low energy electrons (5 GeV). In the present simple conditions the *Total Accordion Correction Factor* is computed by (6) and is shown in figure (8) for various h values and electron energies as a function of the shower depth X. It has been tested that this correction is equivalent to the separate application of the cluster sampling fraction and the out of cone cluster corrections.

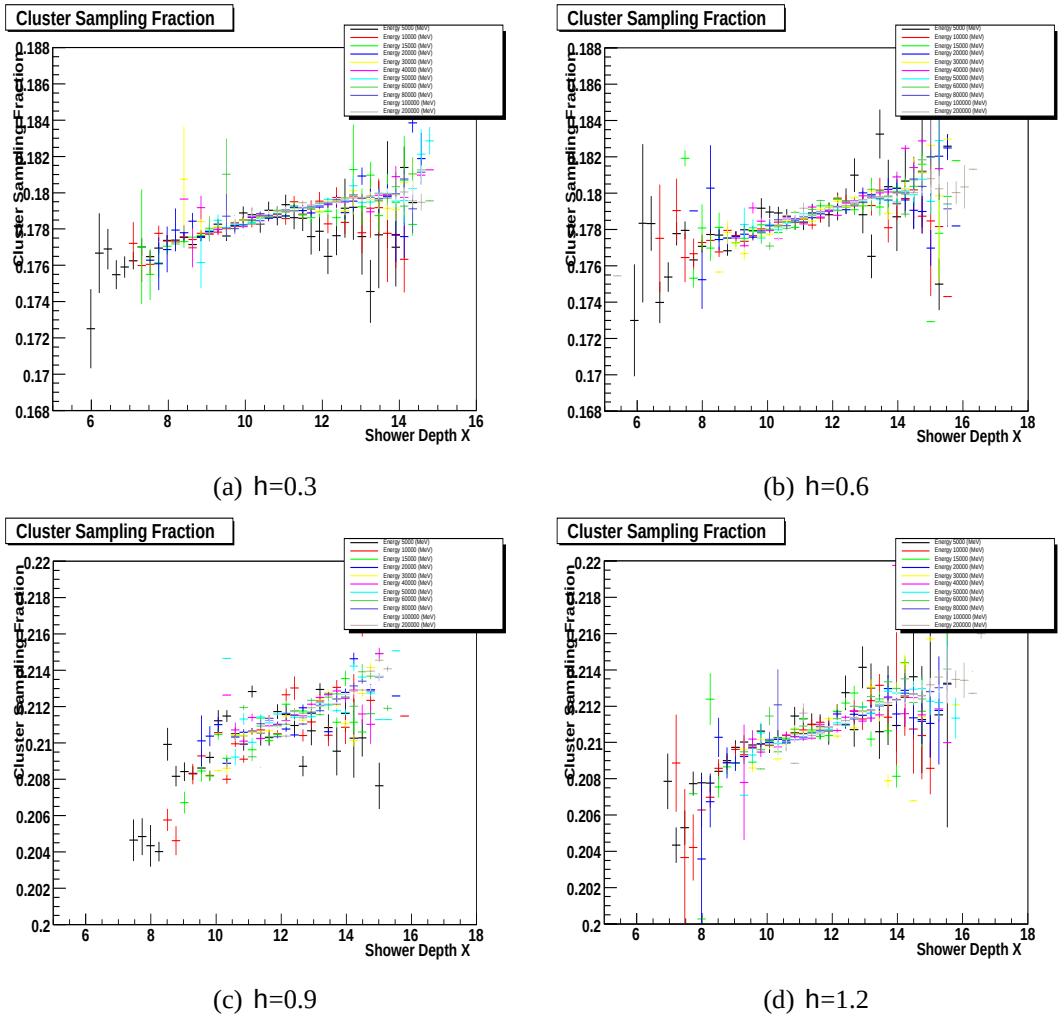

(a) h=0.3 (b) h=0.6

(c) h=0.9 (d) h=1.2

Figure 5: Cluster Sampling Fraction as a function of the shower depth X for various electron energies and h values.

$$Total \quad Accordion \quad Correction \quad Factor = \frac{1}{s_{tot}^{Acc}} = \frac{1}{s_{cl}^{Acc} \cdot f_{out}} \tag{6}$$

This factor is still fairly energy independent. The correction factor averaged over all electron energies is shown in figure 9. It is parametrized as a function of X with a second degree polynomial. In the fit only points with more than 0.5% of the total entries are considered. The large difference between the values at h = 0.3, 0.6 and 0.9, 1.2 is due to the different absorber thickness in these regions of the calorimeter.

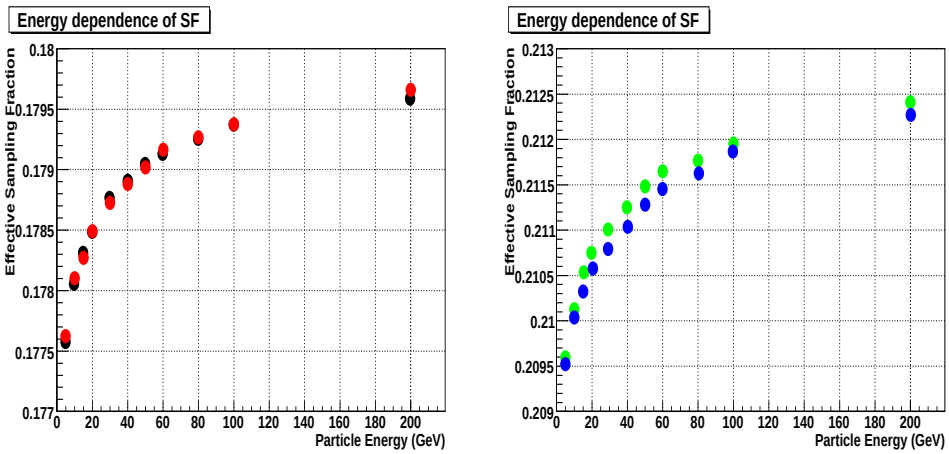

(a) h=0.3 (black) and h=0.6 (red) (b) h=0.9 (green) and h=1.2 (blue)

Figure 6: Energy dependence of the cluster sampling fraction. .

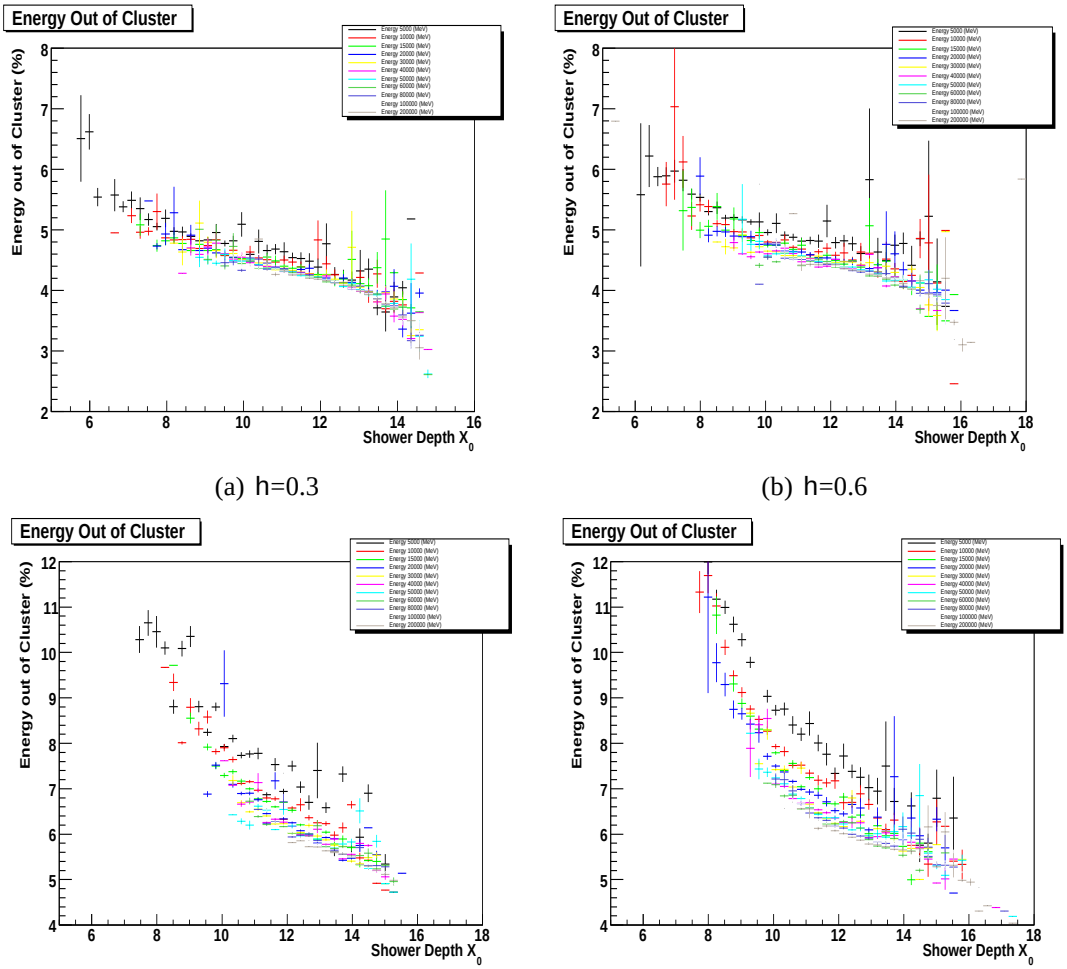

(a) h=0.3 (b) h=0.6

(c) h=0.9 (d) h=1.2

Figure 7: Fraction of energy deposited outside the cluster for various values of electron energy and h.

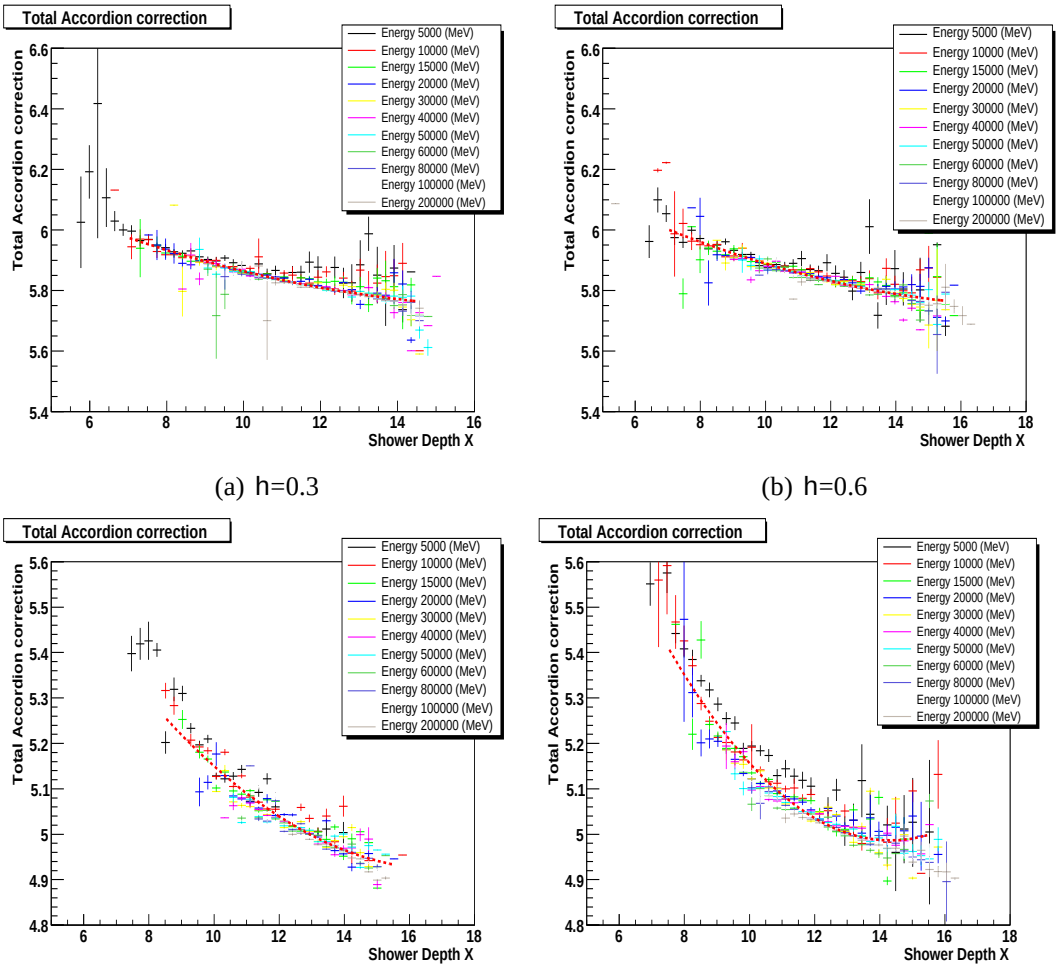

(a) h=0.3 (b) h=0.6

(c) h=0.9 (d) h=1.2

Figure 8: *Total Accordion correction factor* as a function of shower depth X, all energies and various h values. The dashed lines show the parametrization computed on the energy averaged values.

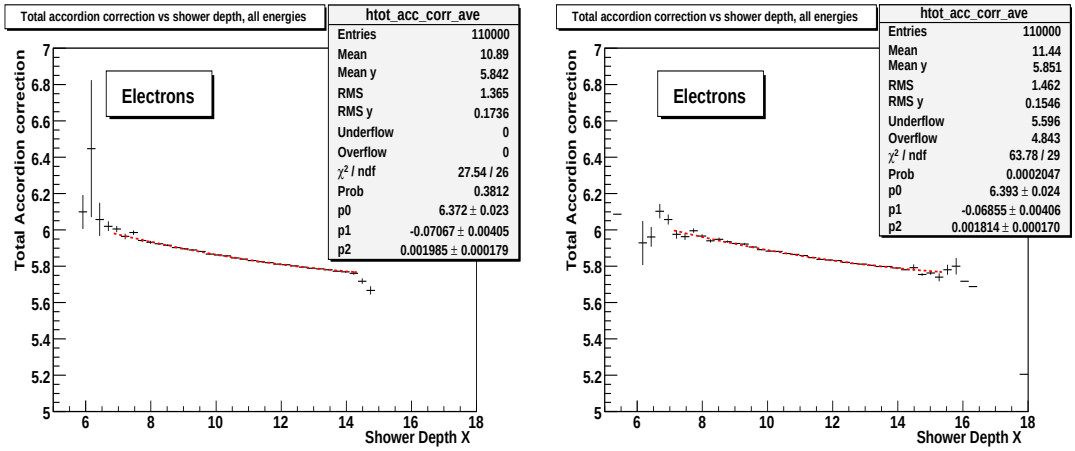

(a) h=0.3 (b) h=0.6

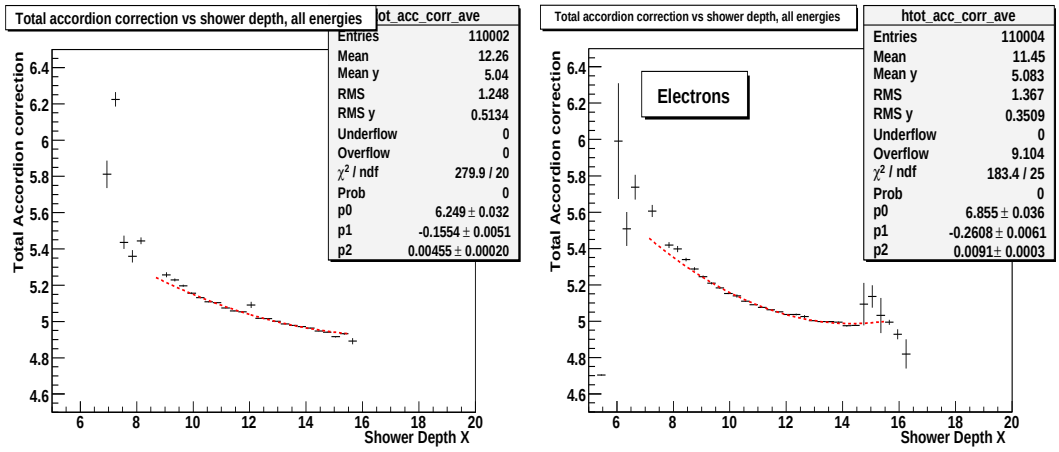

(c) h=0.9 (d) h=1.2

Figure 9: Energy averaged total Accordion correction factor as a function of shower depth X, for various h values. The dashed lines show the results of the parametrization.

4.2 Calculation of the electron energy lost in front of the Accordion

The energy lost in the materials in front of the calorimeter (inner detector, cryostat, coil, materials between preshower and strips...) can be parametrized as a function of the energy lost in the active material of the preshower and is dependent from the electron energy and η as shown in Figures (10),(11),(12) and (13). Note explicitly that the lost energy includes the energy deposited between the preshower and the strips. A separated parametrization of the energy deposited in the inactive and dead materials between preshower and strips as a function of the energy deposited in active materials of the preshower and strips has been tested. Since the energy resolution and the linearity are not improved, to minimize the number of parameters, a parametrization depending only from the energy deposited in the preshower will be used. The use of a first degree polynomial gives good results in term energy resolution and the linearity.

The parameters of the first degree polynomial (labeled *offset* and *slope*) are shown in figure (14) as a function of the mean energy deposited in the Accordion for four η values: 0.3, 0.6, 0.9, 1.2. The dashed lines represent the used parametrization reported in formulas (7) and (8). A non negligible amount of energy is lost before the calorimeter also when no energy is measured in the preshower (offset). This amount increases with the electron energy and is much higher of the energy lost by ionization. We interpret it as due to the absorption of very low energy photons and electrons present in the early shower.

$$a(E_{tot}^{Acc}, \eta) = p_0^{front} + p_1^{front} E_{tot}^{Acc} + p_2^{front} \sqrt{E_{tot}^{Acc}} \tag{7}$$

$$b(E_{tot}^{Acc}, \eta) = p_0^{front} + p_1^{front} \log E_{tot}^{Acc} + p_2^{front} \sqrt{E_{tot}^{Acc}} \tag{8}$$

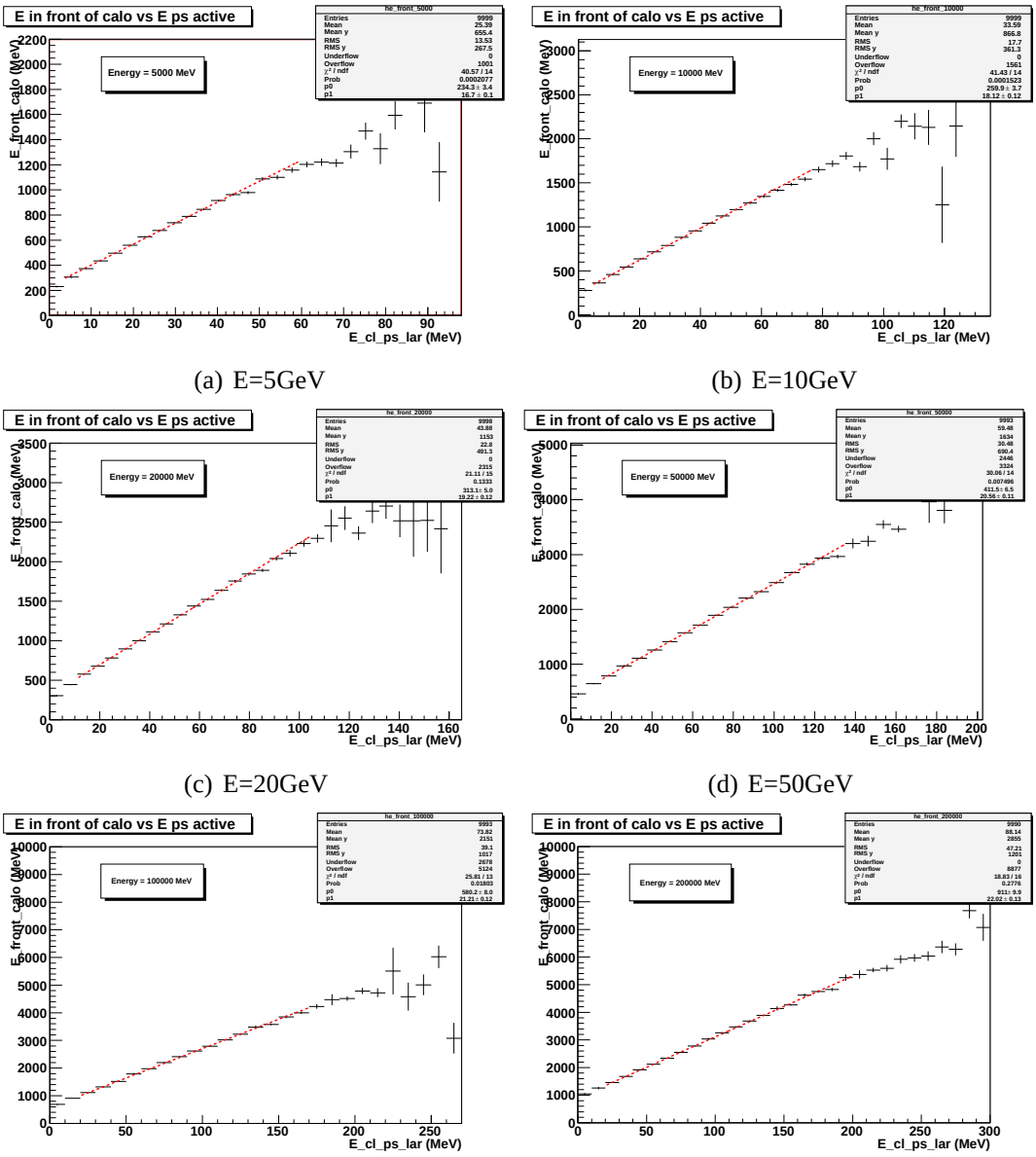

(a) E=5GeV (b) E=10GeV

(c) E=20GeV (d) E=50GeV

(e) E=100GeV (f) E=200GeV

Figure 10: Energy lost in front of the accordion as a function of energy measured in the preshower at h=0.3 for various electron energies. The dashed lines show the linear parametrization.

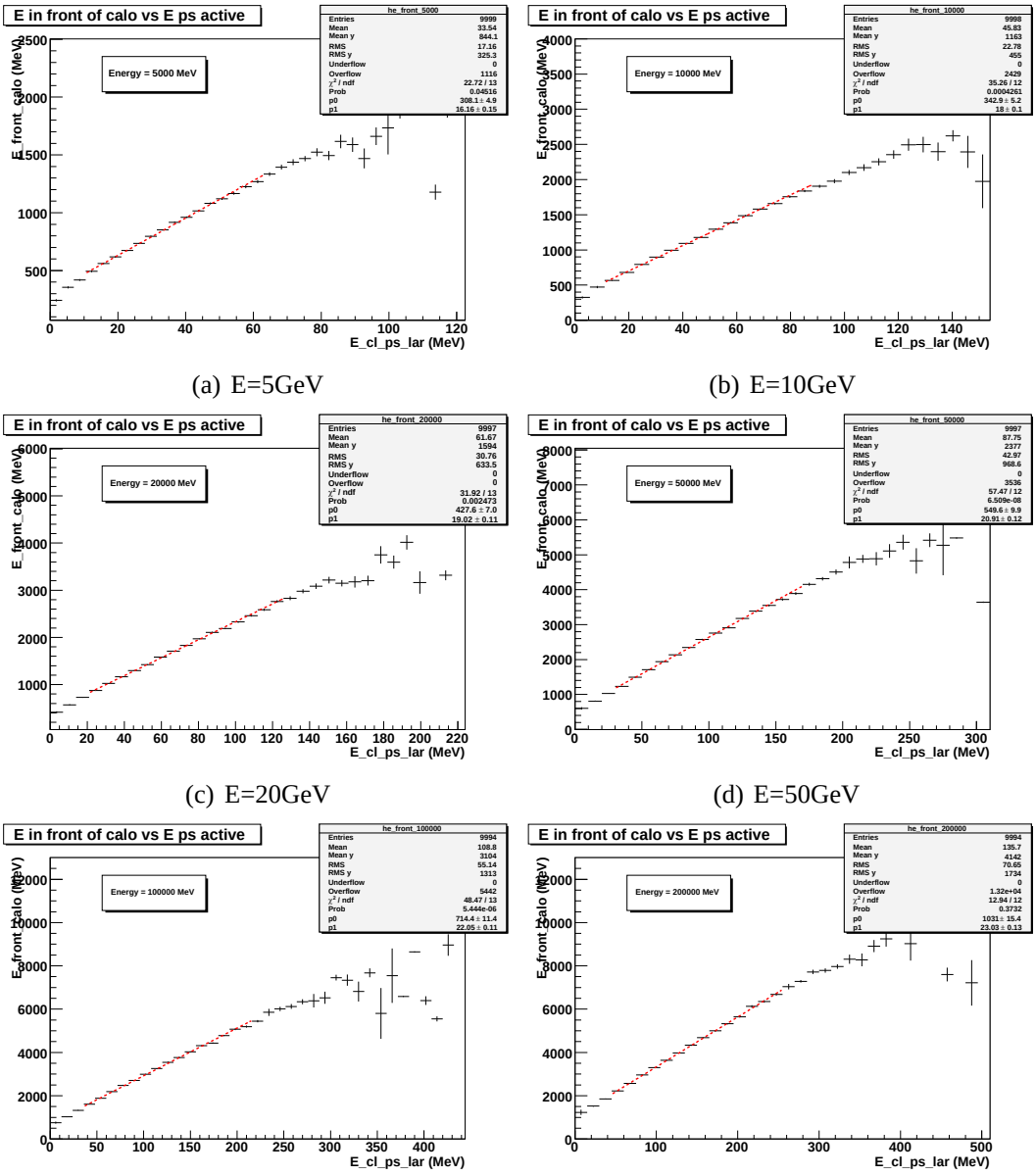

(a) E=5GeV (b) E=10GeV

(c) E=20GeV (d) E=50GeV

(e) E=100GeV (f) E=200GeV

Figure 11: Energy lost in front of the accordion as a function of energy measured in the preshower at h=0.6 for various electron energies. The dashed lines show the linear parametrization.

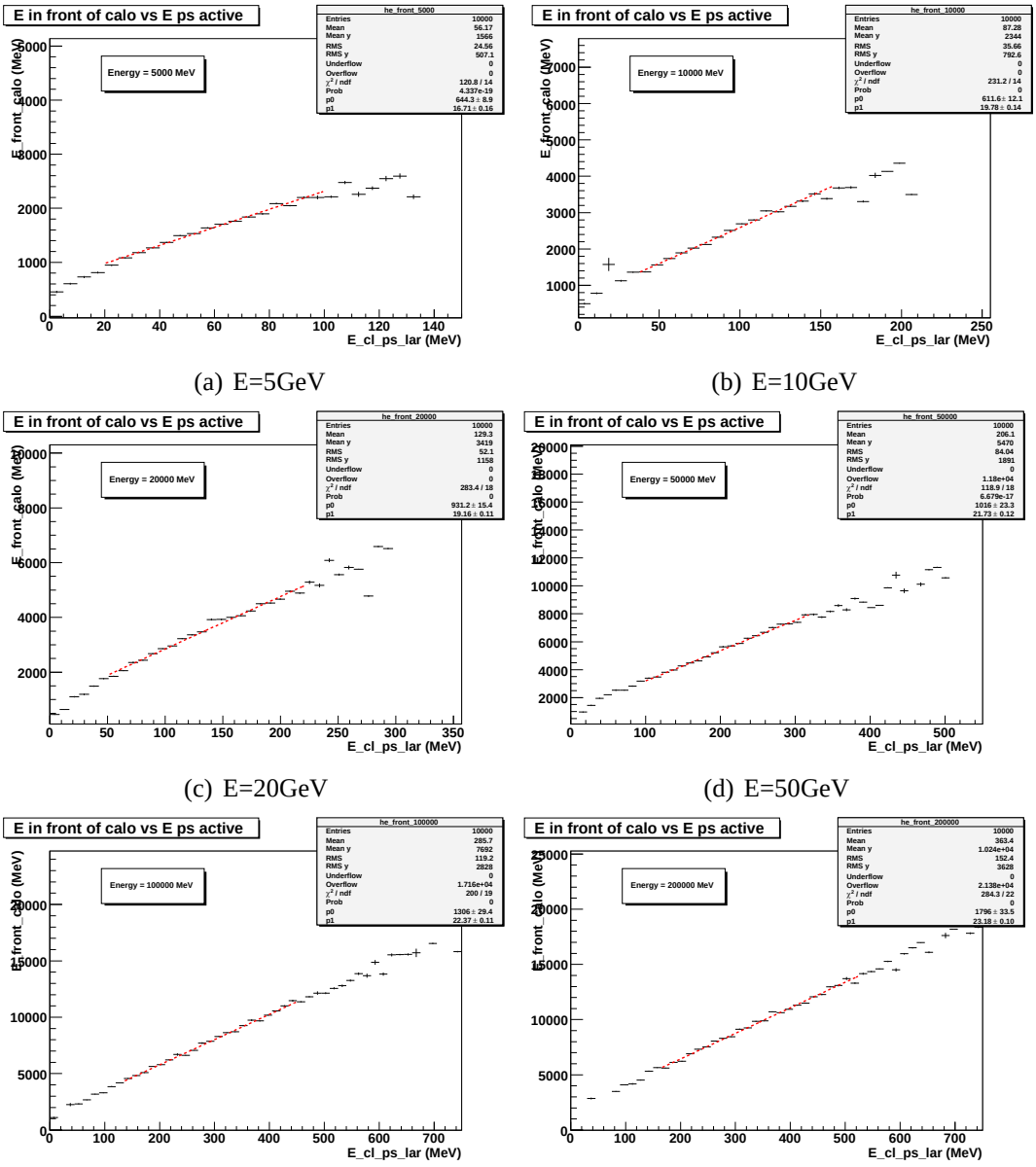

(a) E=5GeV (b) E=10GeV

(c) E=20GeV (d) E=50GeV

(e) E=100GeV (f) E=200GeV

Figure 12: Energy lost in front of the accordion as a function of energy measured in the preshower at h=0.9 for various electron energies. The dashed lines show the linear parametrization.

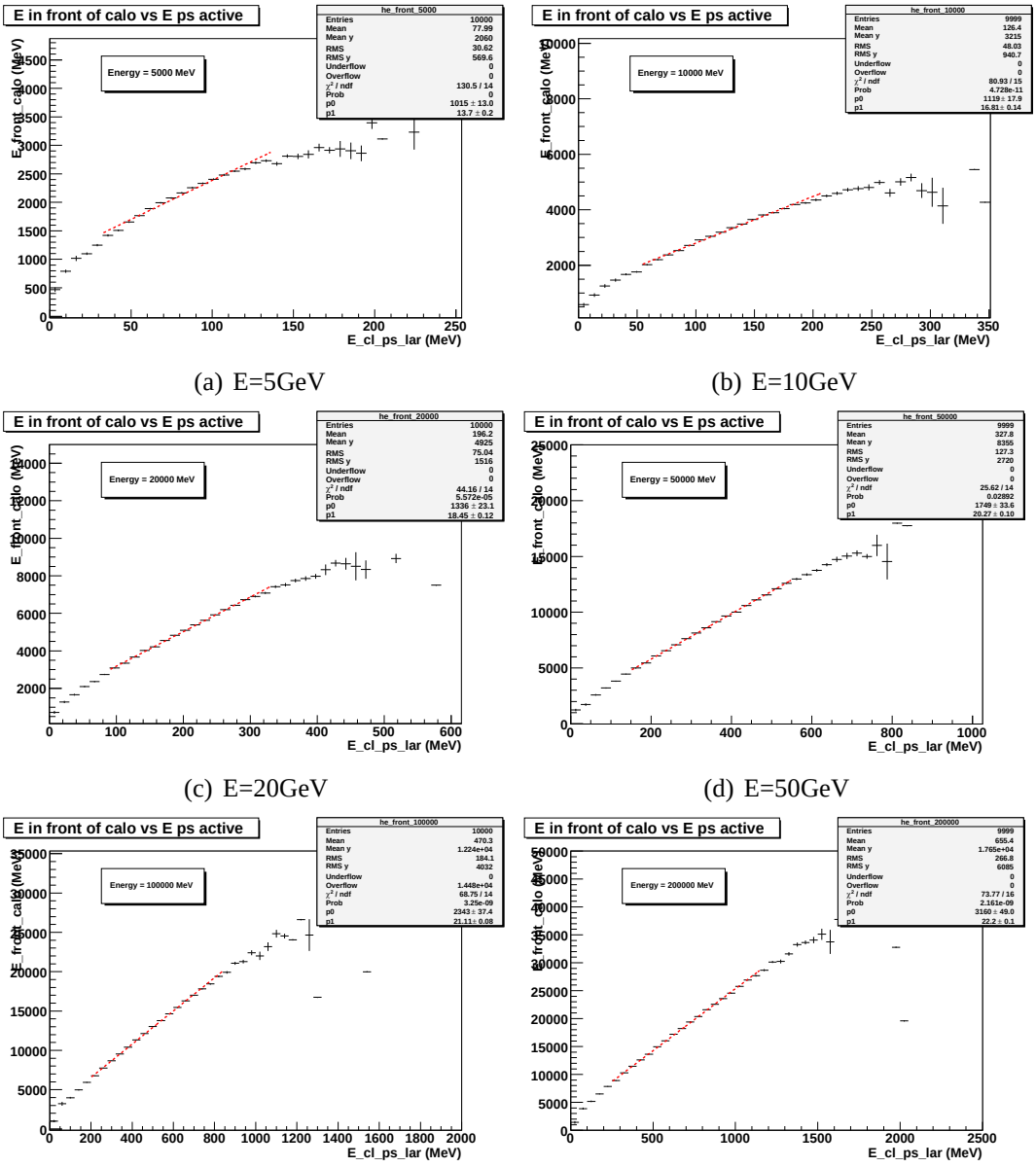

(a) E=5GeV (b) E=10GeV

(c) E=20GeV (d) E=50GeV

(e) E=100GeV (f) E=200GeV

Figure 13: Energy lost in front of the accordion as a function of energy measured in the preshower at h=1.2 for various electron energies. The dashed lines show the linear parametrization.

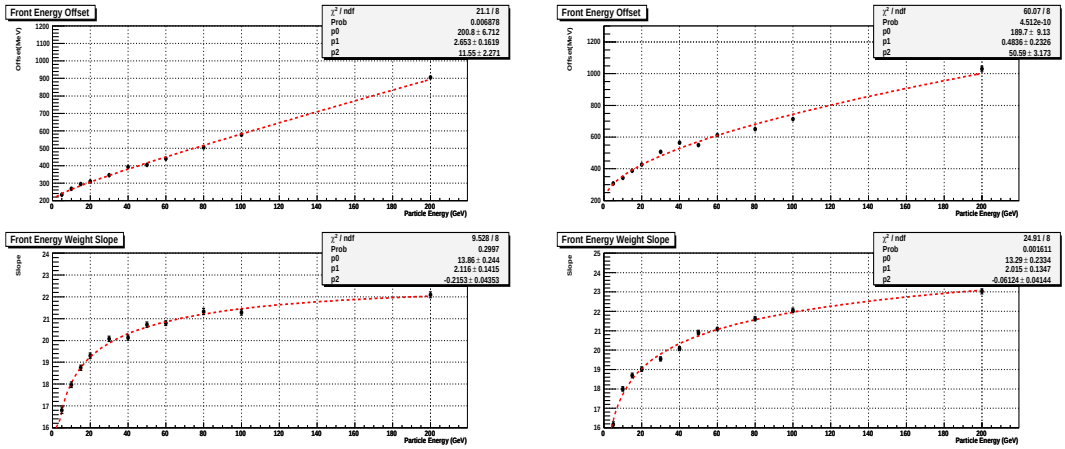

(a) h=0.3 (b) h=0.6

(c) h=0.9 (d) h=1.2

Figure 14: Offset and slope at various eta as a function of the average energy lost in the Accordion. For each h value the top plot is the *offset* and the bottom the *slope*

4.3 Longitudinal leakage correction

The energy deposited by the electron shower behind the Accordion is given as a fraction of the reconstructed energy in the Accordion . As shown in figure (15) for various η values, this fraction, when parametrized as a function of the longitudinal barycenter of the shower X, is fairly energy independent. This fraction, averaged over the electron energies, is parametrized by the equation (9):

$$f_{leak}(\%) = p_0^{leak} X + p_1^{leak} e^X \tag{9}$$

The results of the fits are shown in figure (15) and (16), for four η points. Note that the fraction of energy lost behind the accordion varies at a given X value with η, consistently with the increase of the total radiation length of the calorimeter.

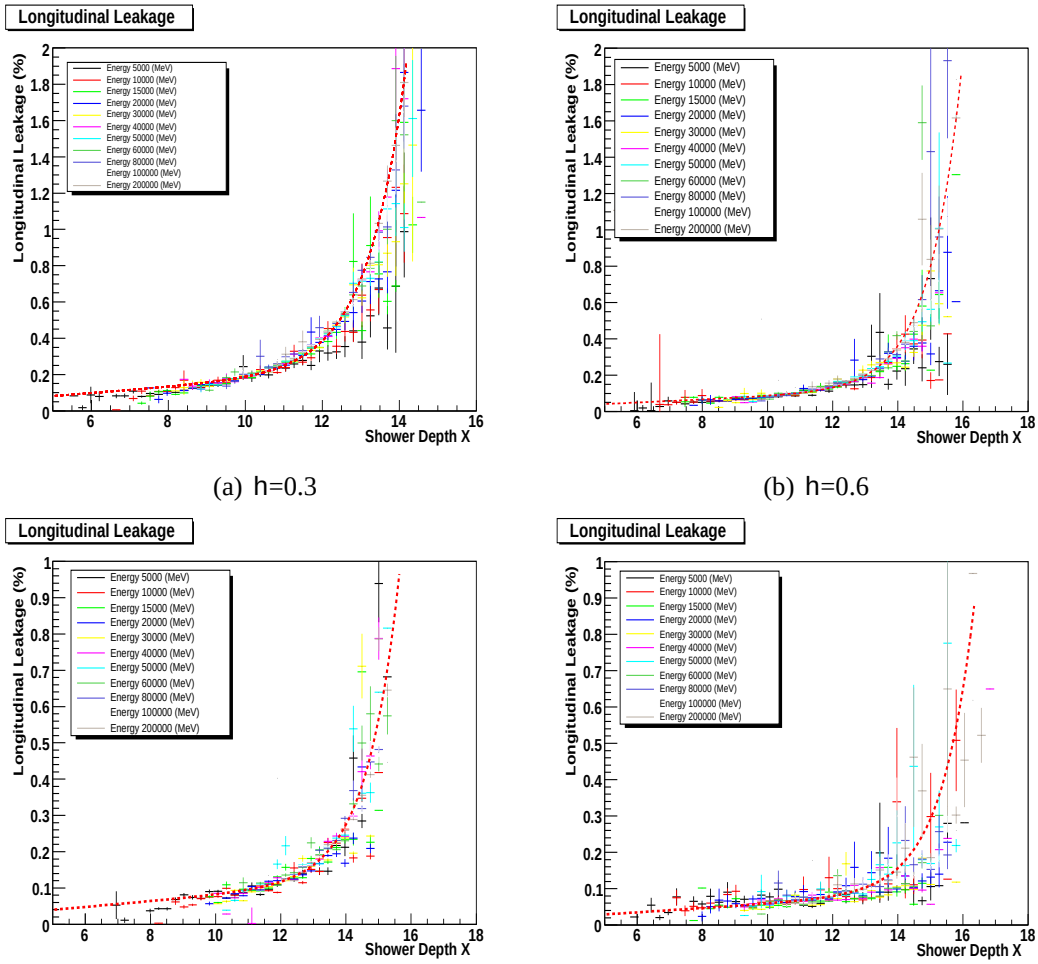

(a) h=0.3 (b) h=0.6

(c) h=0.9 (d) h=1.2

Figure 15: Fraction of the energy deposited behind the Accordion as a function of shower depth X, all energies. The dashed lines show the used parametrization.

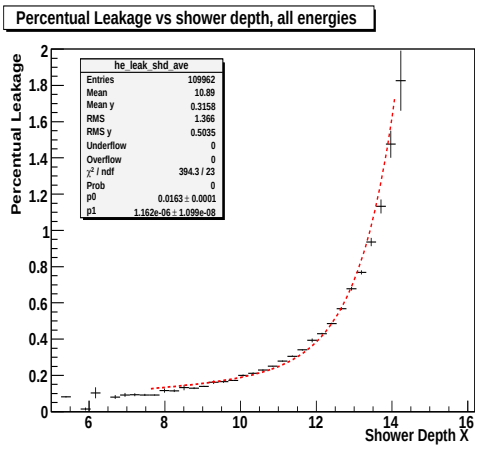

(a) h=0.3

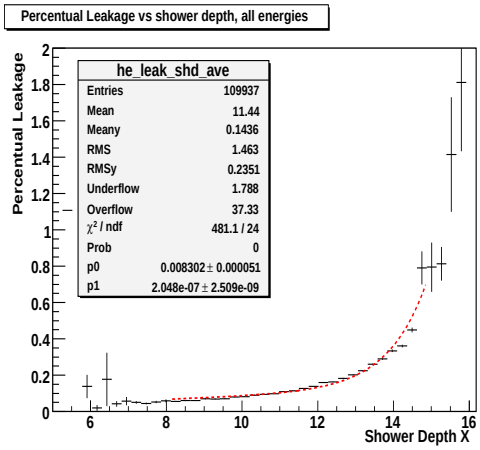

(b) h=0.6

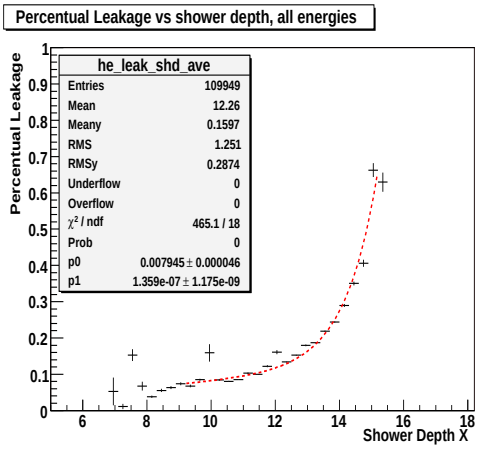

(c) h=0.9

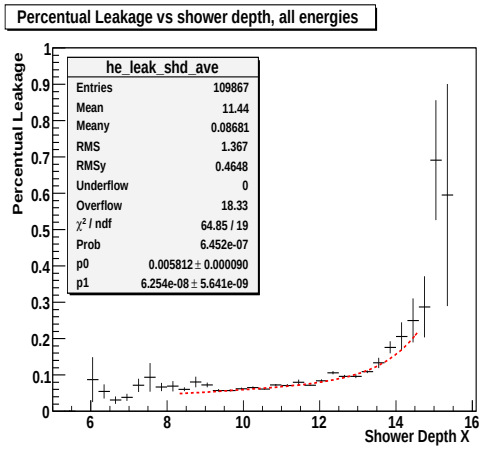

(d) h=1.2

Figure 16: Fraction of energy deposited behind the calorimeter, averaged over the electron energies, as a function of the shower depth X. The used parametrization is superimposed.

4.4 Resolution and Linearity

The electron energy has been computed with the described method. As an example in figure (17) the energy profiles of various electron samples at η= 0.3 are shown. From a fit with a gaussian in the interval $[-2\sigma, +2\sigma]$ mean values and standard deviations are obtained. As usual the energy resolution $\frac{\sigma(E)}{E}$ (labeled *resolution*) is parametrized as:

$$\frac{\sigma(E)}{E} = \frac{b}{\sqrt{E(MeV)}} \oplus c \tag{10}$$

where: b is the sampling and c is the constant term of the calorimeter.

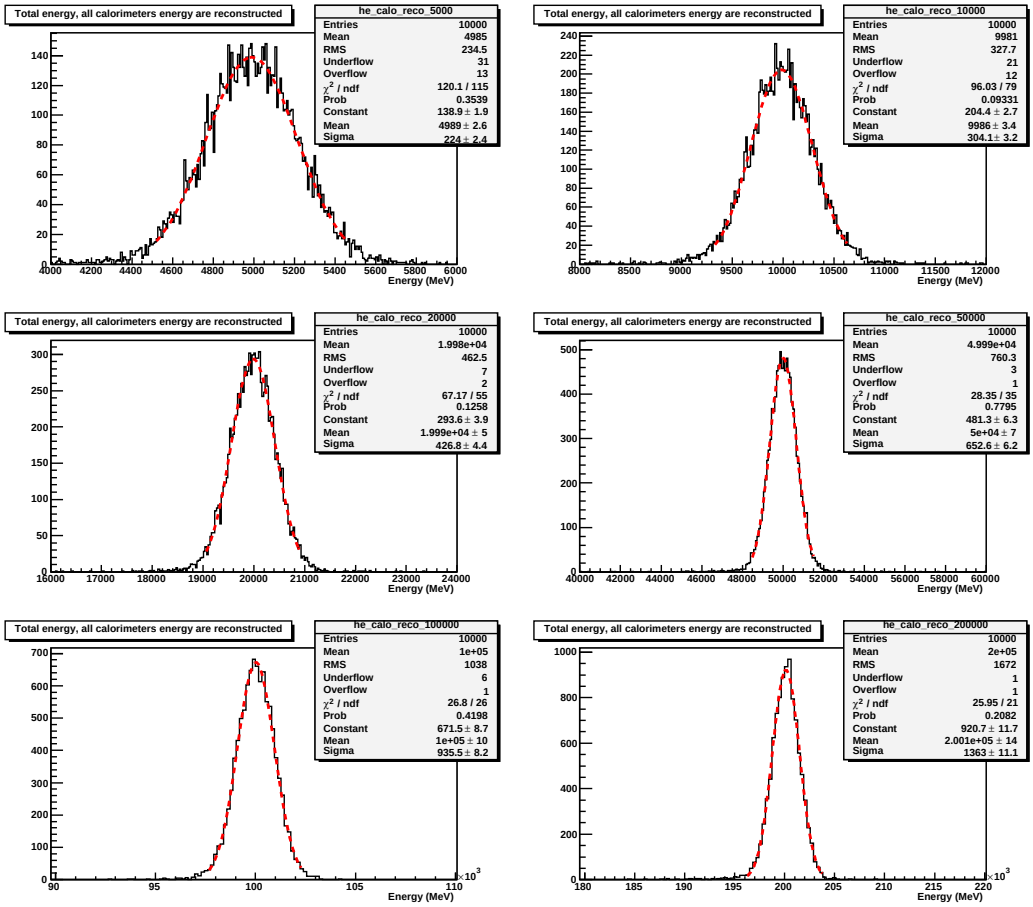

Figure 17: Total reconstructed electron energy at η=0.3, centre cell

The resolution, the sampling and the constant terms are shown in figures (18) for η=0.3, 0.6, 0.9, 1.2. The black points show the results when all contributions

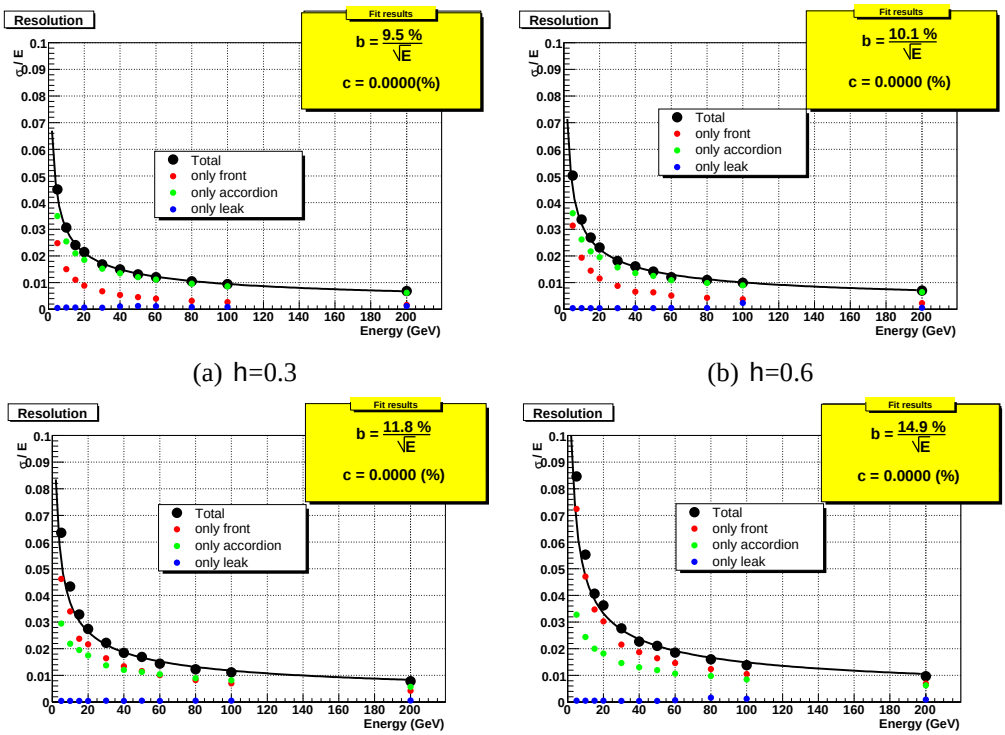

(a) h=0.3 (b) h=0.6

(c) h=0.9 (d) h=1.2

Figure 18: Resolution for various h points. The meaning of the different points is explained in the text.

to the electron energy are computed with the described method. Results when only the energy in the Accordion is computed while all other contributions are assumed from the Monte Carlo simulation are shown with the green points. The red and the blue points refer respectively to the case in which the only computed energies are the energy lost in front and behind the calorimeter.

Values of the sampling and the constant term as a function of h are listed in table (1).

Note that the constant term of the energy resolution is zero at all h points, as expected for a simulation at the cell centre. The sampling term increases from 8.7% at low h values to 15 % at h= 1.2. This is related to the increase of the energy lost in front of the calorimeter. Note also that while for h less than 0.8 the dominant contribution to the energy resolution comes from the Accordion, for h larger than 0.8 the dominant contribution comes from the energy deposited in front of it as shown in figure (20). The difference of the fitted mean value and true electron energy (labeled *linearity*) is shown in figure (19). The meaning of the different colours is the same as in figure (18) and is explained above in the text.

h_{cell}	b(%)	c	Linearity (%)
0.1	8.7	0	0.1
0.2	8.9	0	0.1
0.3	9.5	0	0.1
0.4	9.6	0	0.1
0.5	9.9	0	0.1
0.6	10.1	0	0.2
0.7	11.3	0	0.2
0.9	11.8	0	0.3
1.0	12.9	0	0.4
1.1	13.8	0	0.4
1.2	14.9	0	0.4

Table 1: Sampling term, constant term and linearity at various h values

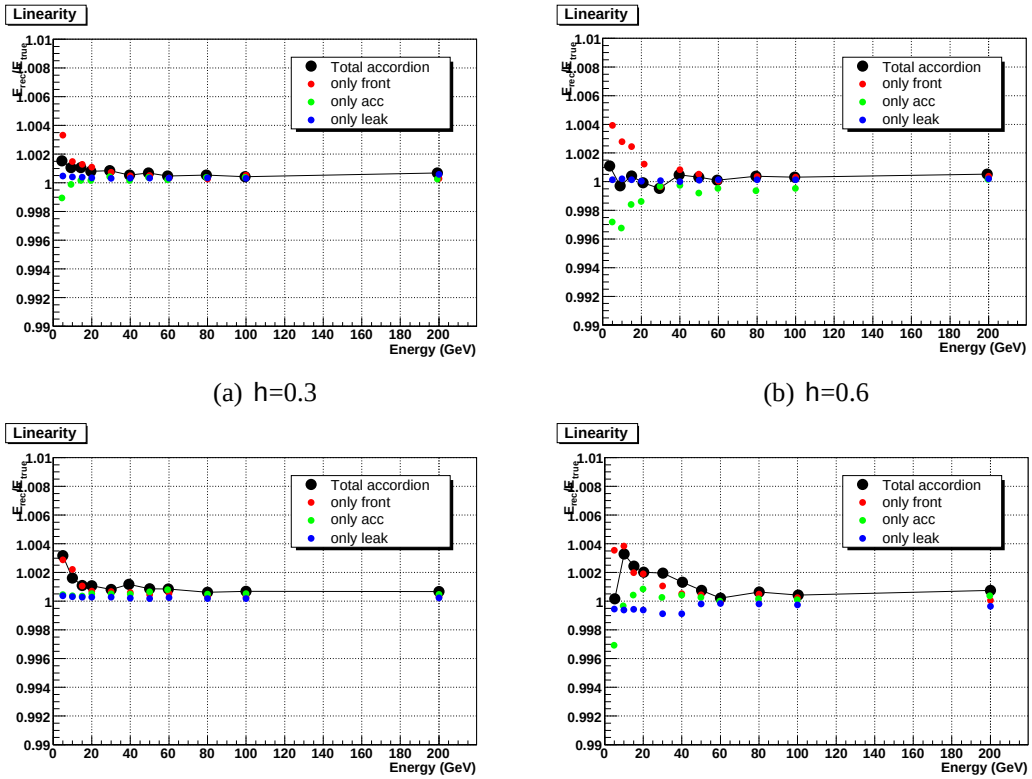

(a) h=0.3 (b) h=0.6

(c) h=0.9 (d) h=1.2

Figure 19: Linearity for various h values.

The maximum absolute value of the linearity is listed in table (1).

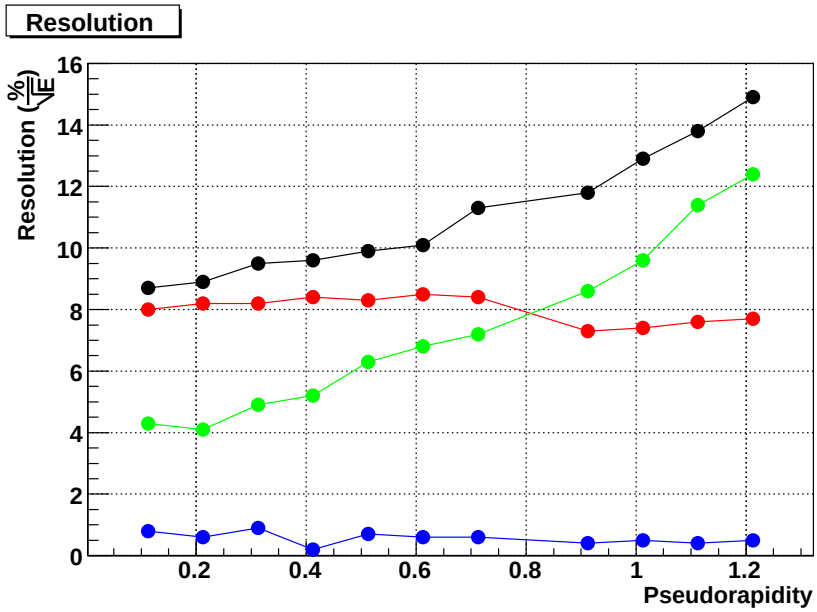

Figure 20: Sampling term versus h

5 Electrons hitting uniformly a cell of the middle compartment

In this section the results obtained with the previous method have been tested when the electrons hit uniformly a middle cell. In addition the corrections to be applied as a function of the impact position have been studied. The method holds also in this situation.

The computation of the electron energy strictly follows the procedure shown in the previous paragraph. Here we simply discuss the obtained results.
The *Total Accordion Correction Factor* averaged over all energies is shown in figure (21) for h= 0.3 and h= 1.2 as a function of the shower depth X .

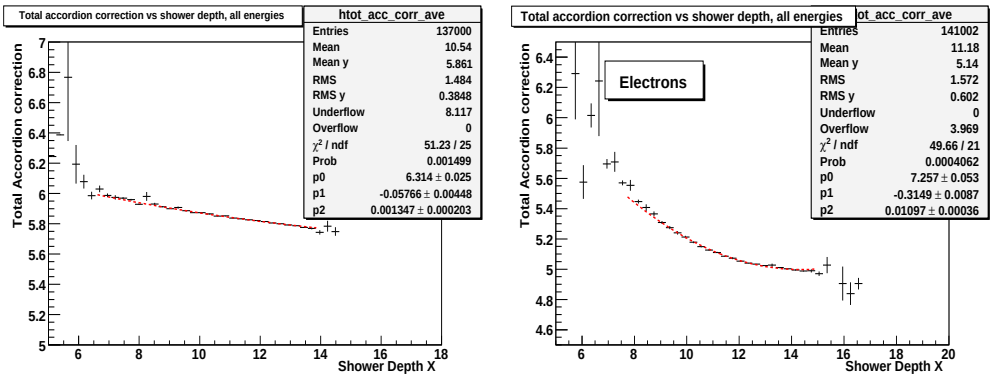

(a) h=0.3 (b) h=1.2

Figure 21: Total Accordion Correction Factor averaged over all energies as a function of Shower Depth X. The results of the used parametrization are superimposed as dashed red lines in the interval used in the fit

The energy deposited in the material in front of the calorimeter is parametrized as a function of the energy measured in the active material of the preshower as before. In figure (22) and (23) the energy deposited in front of the calorimeter is shown as a function of the energy measured in the preshower for various energies. The results of the used linear parametrization are superimposed in the interval used in the fit.

The parameters of the parametrization (*offset* and *slope*) are shown in figure (24) as a function of the mean energy deposited in the Accordion. The two top plots show the offset and the slope at h = 0.3. The two bottom plots refer to h = 1.2. The result of the parametrization are superimposed.

The energy lost behind the Accordion is reconstructed and parametrized in the same way as in the centre of cell case. In figure (25) the ratio between the energy deposited behind the Accordion and the energy deposited in the Accordion,

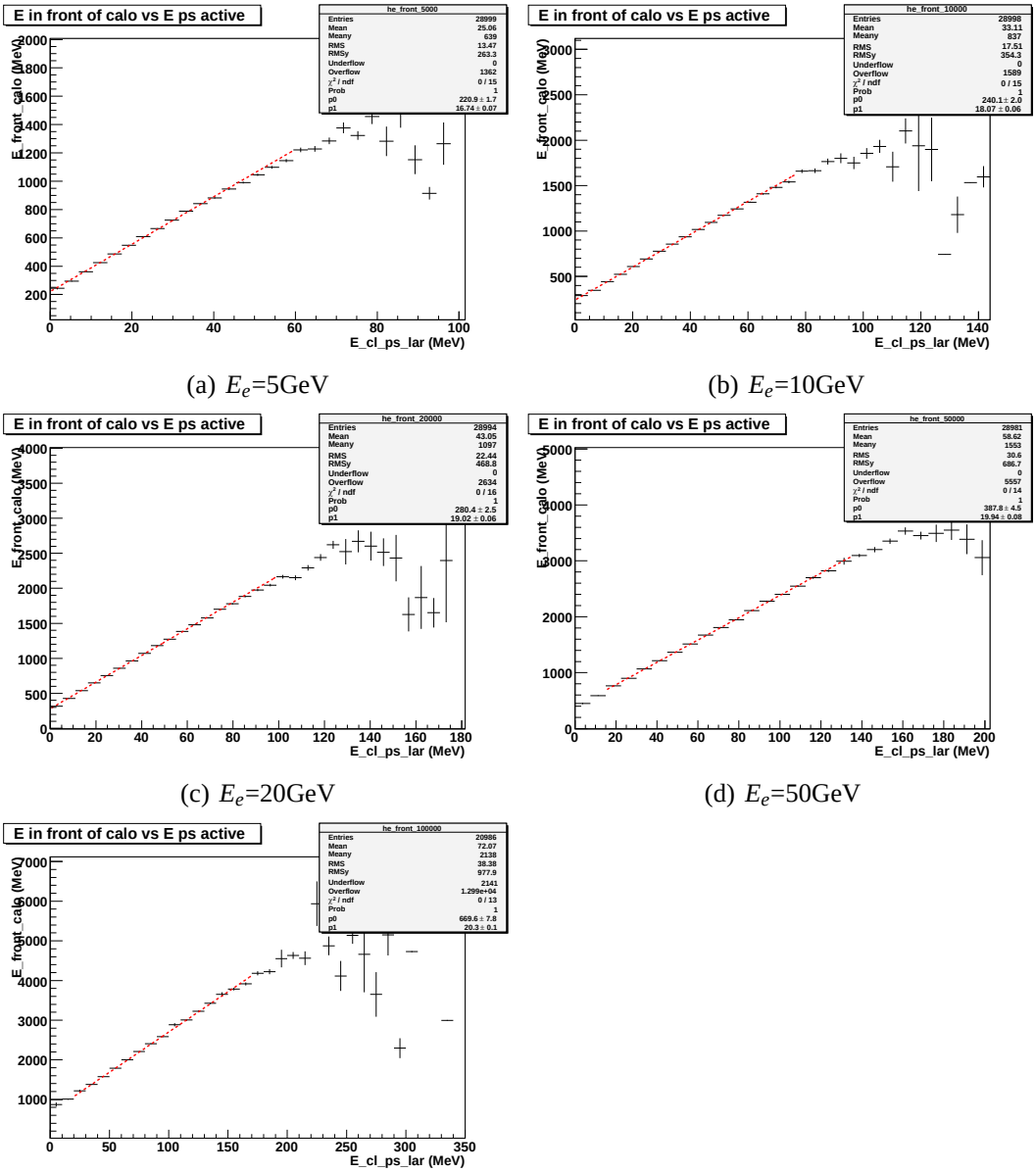

(a) E_e=5GeV

(b) E_e=10GeV

(c) E_e=20GeV

(d) E_e=50GeV

(e) E_e=100GeV

Figure 22: Energy deposited in front of the Accordion as a function of energy deposited in the preshower at h= 0.3 for various energies. The results of the used parametrization are superimposed as dashed red lines in the interval used in the fit.

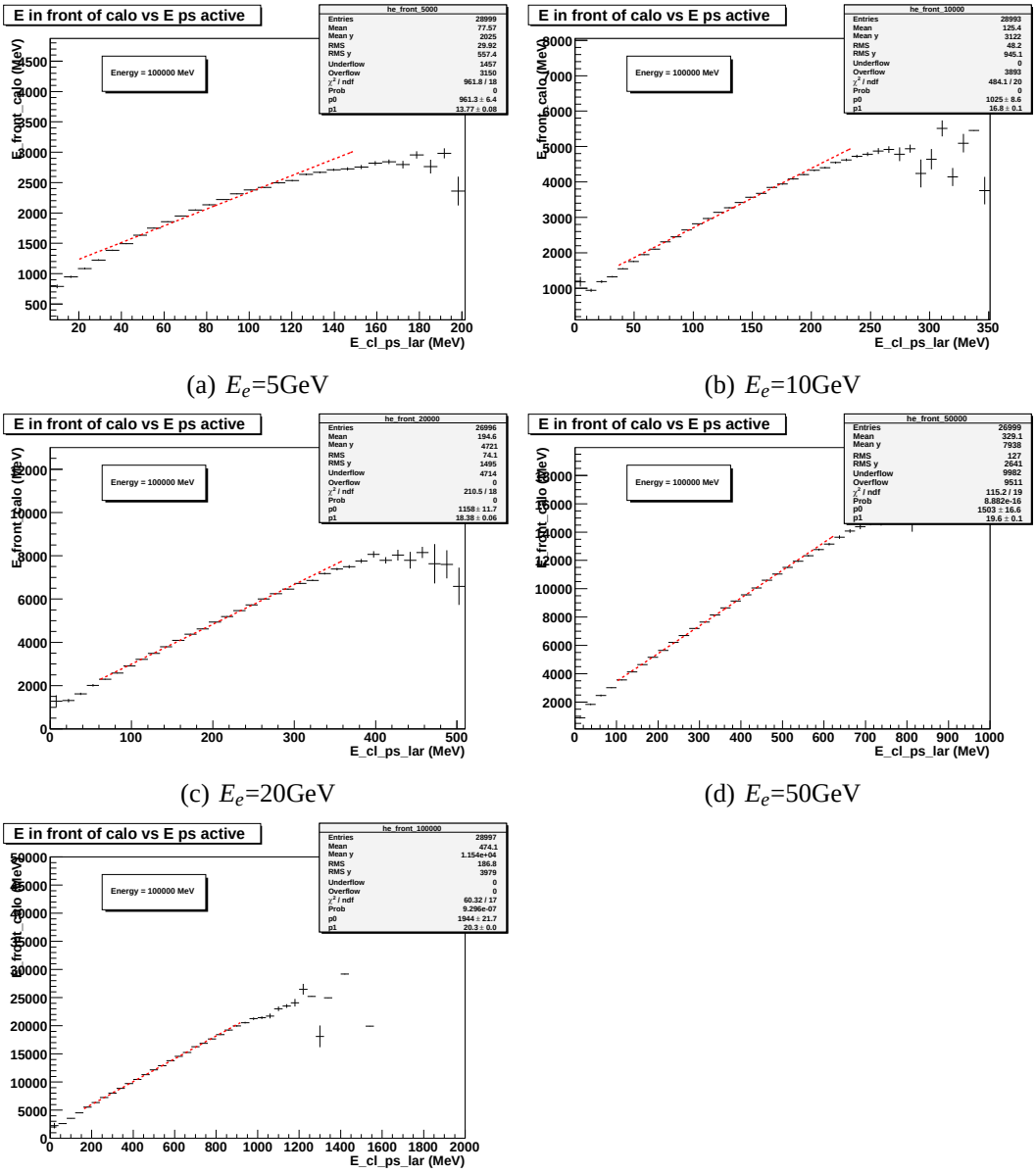

(a) E_e=5GeV

(b) E_e=10GeV

(c) E_e=20GeV

(d) E_e=50GeV

(e) E_e=100GeV

Figure 23: Energy deposited in front of the Accordion as a function of energy deposited in the preshower at h= 1.2 for various energies. The results of the used parametrization are superimposed as dashed red lines in the interval used in the fit.

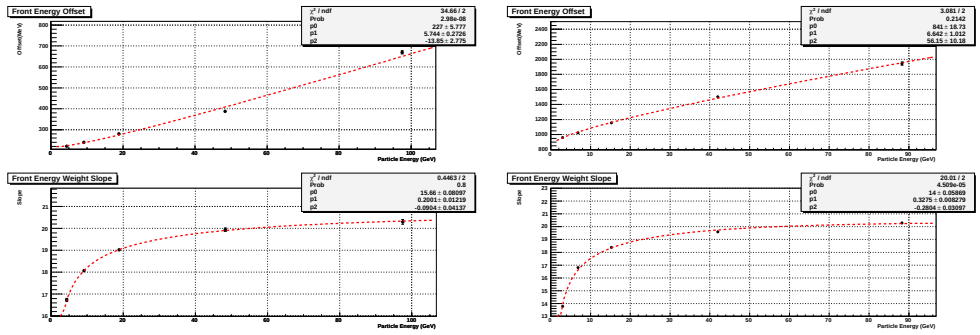

(a) h=0.3 (b) h=1.2

Figure 24: Offset and slope as a function of the mean energy deposited in the Accordion. For each h value the top plot refers to the offset, the bottom to the slope. The results of the parametrization are superimposed as red dotted lines.

averaged over all electron energies as a function of *Shower Depth X* is shown with the results of the used parametrization.

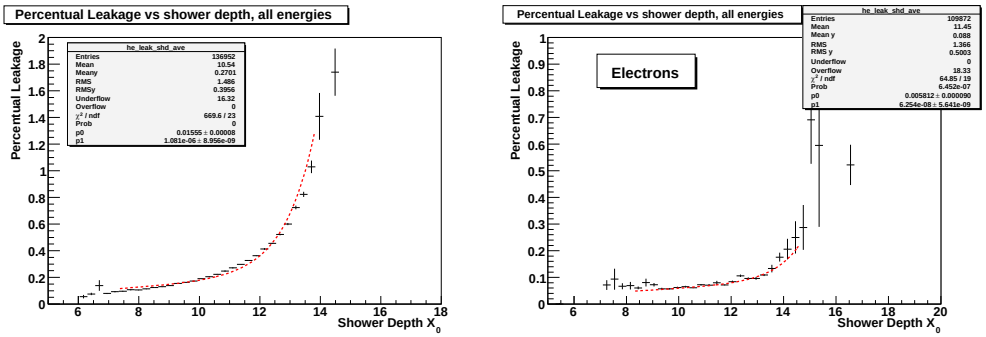

(a) h=0.3 (b) h=1.2

Figure 25: Ratio between the energy deposited behind the Accordion and the energy deposited in the Accordion averaged over all electron energies as a function of shower depth X. The results of the used parametrization are superimposed as dotted red lines.

5.1 Resolution and Linearity

The obtained energy resolution and linearity are show respectively in figures (26) and (27) and listed in table (2).
The sampling term and the linearity values are similar to the ones obtained for the electrons hitting the cell centre, but now the constant term of the resolution is about 0.2-0.3 %. This is due to the fact that the energy deposited in the Accordion

depends from the the impact point of the electron inside a cell and this dependence is not taken into account. The dependence of the computed electron energy from the impact point in a cell is partly outside the aim of this work. However for completeness some studies were done and the results will be reported and discussed in the next section.

h_{cell}	b(%)	c	Linearity (%)
0.3	9.8	0.3	0.1
0.6	10.6	0.2	0.2
0.7	12.1	0.2	0.3
1.0	14.1	0.3	0.3
1.1	15.5	0.2	0.4
1.2	17.6	0.2	0.5

Table 2: Electrons spread over a cell of the middle compartment.Resolution and Linearity before h and f modulations correction

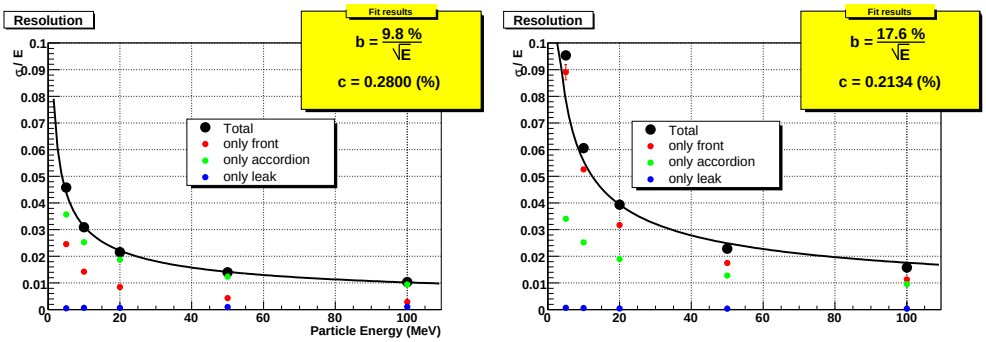

(a) h=0.3 (b) h=1.2

Figure 26: Electrons spread over a cell of the middle compartment. Energy resolution before h and f modulation correction.

5.2 Computation of the impact position

From the calorimeter information the electron impact point is computed as the barycentre of the cluster, defi ned by the equation (11).

$$x_{bary} = \frac{\sum_i^{cluster} E_i x_i}{\sum_i^{cluster} E_i} \tag{11}$$

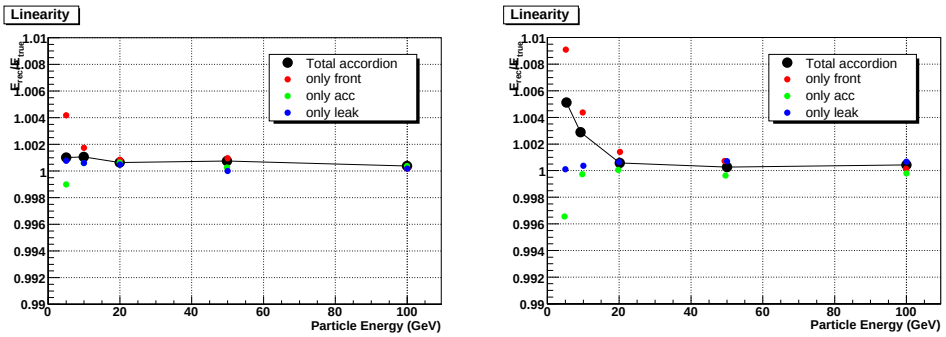

(a) h=0.3 (b) h=1.2

Figure 27: Electrons spread over a cell of the middle compartment. Linearity before h and f modulation correction.

Where x_i is either the h or the f value at the center of the middle compartment of the cell i of the cluster. Only the middle compartment is considered due to the granularity in f of the strips.

As an example in fi gure (28) the true versus the computed h and f at h = 0.3 are shown for all electron energies.

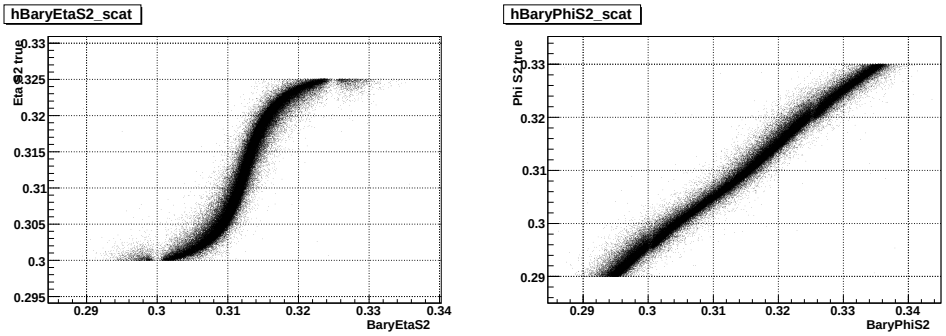

(a) h (b) f

Figure 28: h and f simulated values versus the h and f barycentre values (middle compartment). All simulated electron energies superimposed.

In fi gure (29) the difference between the simulated and the reconstructed f (h = 0.3) shows the presence of an offset value. No signifi cant offset is present in the analogous h distribution. The same conclusions are valid for all studied h values.

Table (3) gives the offset values for the f coordinate at few h points. The offset is due to the Accordion shape and depends from the beginning in depth of the middle compartment respect to the folds of the absorbers and electrodes. The offset is h dependent since it follows the varying strip length.

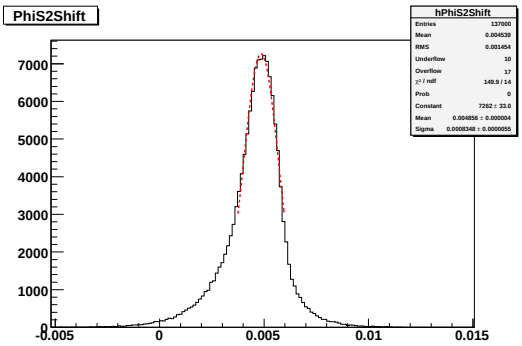

Figure 29: Difference between simulated and reconstructed ϕ barycentre in the middle compartment for all simulated electron energies at $\eta = 0.3$

η_{cell}	0.3	0.6	0.7	1.0	1.1	1.2
ϕ_{middle}^{offset}	0.19	0.19	0.18	0.26	0.27	0.30

Table 3: ϕ_{middle}^{offset} , expressed in unity of the middle cell.

Figure (30) shows the difference between the true and the reconstructed η value in the middle compartment, as a function of the computed η position in normalized cell unit for various electron energies. This behavior, usually labeled as *S-Shape*, originates from the cell granularity and the shower lateral profile in the middle compartment and is a function of the electron energy and η. The correction to be applied to the reconstructed position varies with the electron energy for less than10% of the cell width. Since in the next paragraph it will be shown that the correction to the electron energy does not strongly depend from the position in the cell, the dependence of the correction on the position from the electron energy is neglected and a correction averaged over all electron energies is applied.

The difference, averaged over all electron energies, between the simulated and the reconstructed η in the middle compartment, normalized to the η width of the cell is shown in Figure (31) and parametrized as :

$$\frac{\eta_{bary} - \eta_{true}}{\Delta\eta_{cell}} = p_0 \cdot \arctan(p_1 \cdot \eta_{bary}) + p_2 \cdot \eta_{bary} + p_3 \qquad (12)$$

The various coefficients are given in table (4) for various η values.

5.3 Dependence of the electron energy from the impact point

The energy deposited in the Accordion depends also from the impact point of the electron inside the cell.

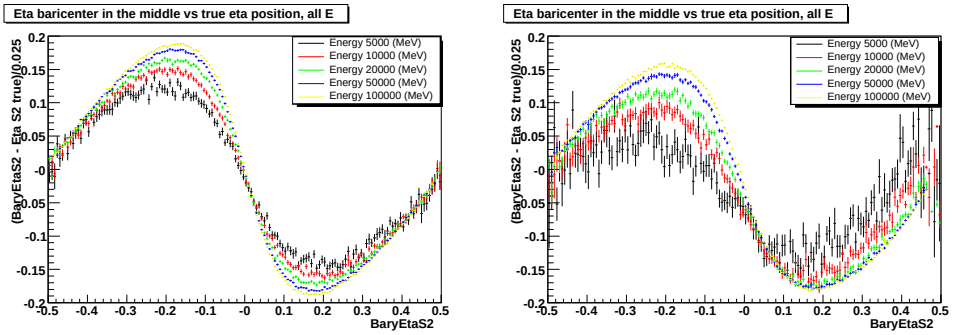

(a) h=0.3 (b) h=1.2

Figure 30: The difference between the simulated and the reconstructed h values in the middle compartment for various electron energies versus the computed h position in normalized cell units.

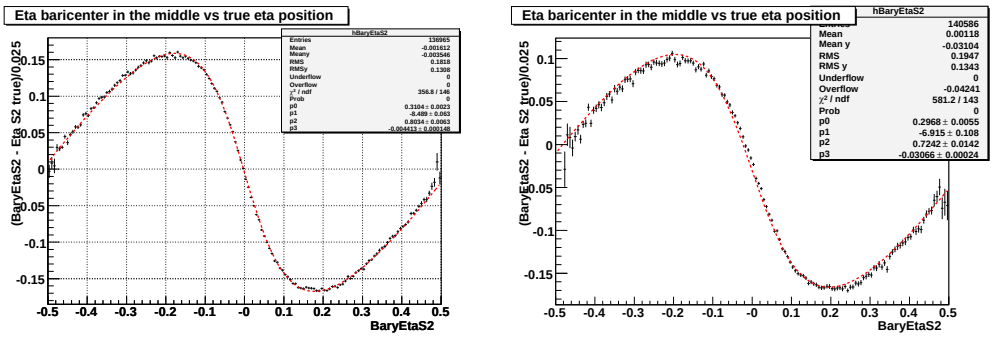

(a) h=0.3 (b) h=1.2

Figure 31: The difference between the simulated and the reconstructed h values in the middle compartment averaged over the electron energies versus the computed h value in normalized cell units. The red dashed line is the result of the proposed parametrization.

η_{cell}	p_0	p_1	p_2	p_3
0.3	0.310 ± 0.002	-8.49 ± 0.06	0.803 ± 0.006	-0.0044 ± 0.0001
0.6	0.306 ± 0.003	-8.6 ± 0.10	0.793 ± 0.007	-0.0107 ± 0.0002
1.0	0.294 ± 0.004	-8.19 ± 0.09	0.75 ± 0.01	-0.0204 ± 0.0002
1.1	0.277 ± 0.004	-7.93 ± 0.11	0.69 ± 0.01	-0.0257 ± 0.0002
1.2	0.297 ± 0.005	-6.9 ± 0.1	0.72 ± 0.01	-0.0306 ± 0.0002

Table 4: S-Shape correction parameters, averaged over the simulated electron energies, for various η values .

In figure (32) and (33) the ratio between the electron reconstructed energy and the nominal energy value is shown as a function of the impact point of the electron in normalized η cell unit. In the following this effect will be called *energy* η *modulation*.

This ratio is parametrized with a second order polynomial, like in equation (13).

$$\frac{E_{reco}}{E_{true}} = p_0 + p_1 \cdot \eta_{cell} + p_2 \cdot \eta_{cell}^2 \tag{13}$$

As an example the computed coefficients are listed in table (5) for η= 0.3.

The dependence of the correction, as tested, from the electron energy is negligible and we will use a parametrization averaged on the electron energies. As an example the electron energy averaged values and the results of the parametrization are shown in figure (34) for η =0.3 and η= 1.2 .

$Energy(GeV)$	p_0	p_1	p_2
5GeV	1.001	-1.1E-03 $\pm$ 0.99E-03	-35.6E-03 $\pm$ 4E-03
10GeV	1.001	-0.8E-03 $\pm$ 0.69E-03	-29.5E-03 $\pm$ 2.72E-03
20GeV	1.001	-1.2E-03 $\pm$ 0.49E-03	-28.6E-03 $\pm$ 1.94E-03
50GeV	1.001	-0.4E-03 $\pm$ 0.34E-03	-27.8E-03 $\pm$ 1.31E-03
100GeV	1.002	-0.3E-03 $\pm$ 0.31E-03	-26.3E-03 $\pm$ 1.1E-03
Averaged	1.002	-0.6E-03 $\pm$ 0.31E-03	-30.5E-03 $\pm$ 1.21E-03

Table 5: *Energy* η *modulation* parameters of formula (13) at η=0.3. The last line lists the values of the parameters computed after averaging on simulated electron energies.

As shown in figure (35) and (36) the reconstructed electron energy depends also from the ϕ value of the impact point inside a cell *(Energy* ϕ *modulation).* The clearly seen four-fold symmetry reflects the absorber periodicity in ϕ inside a cell.

The ratio between the reconstructed electron energy and the nominal one is

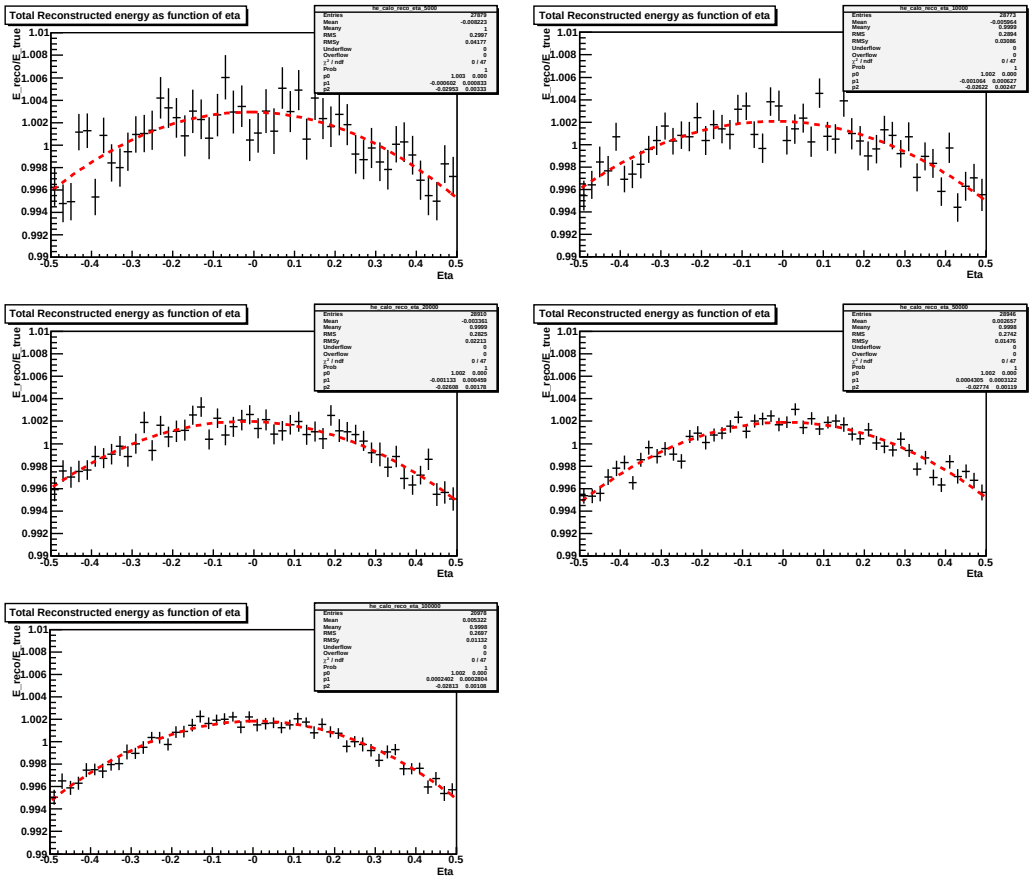

Figure 32: Ratio of the reconstructed energy and the simulated energy as a function of the impact point inside the cell (*energy* h *modulation*) in normalized h cell units at h= 0.3. From left to right and top to bottom 5, 10, 20, 50 and 100 GeV electron energies are shown.

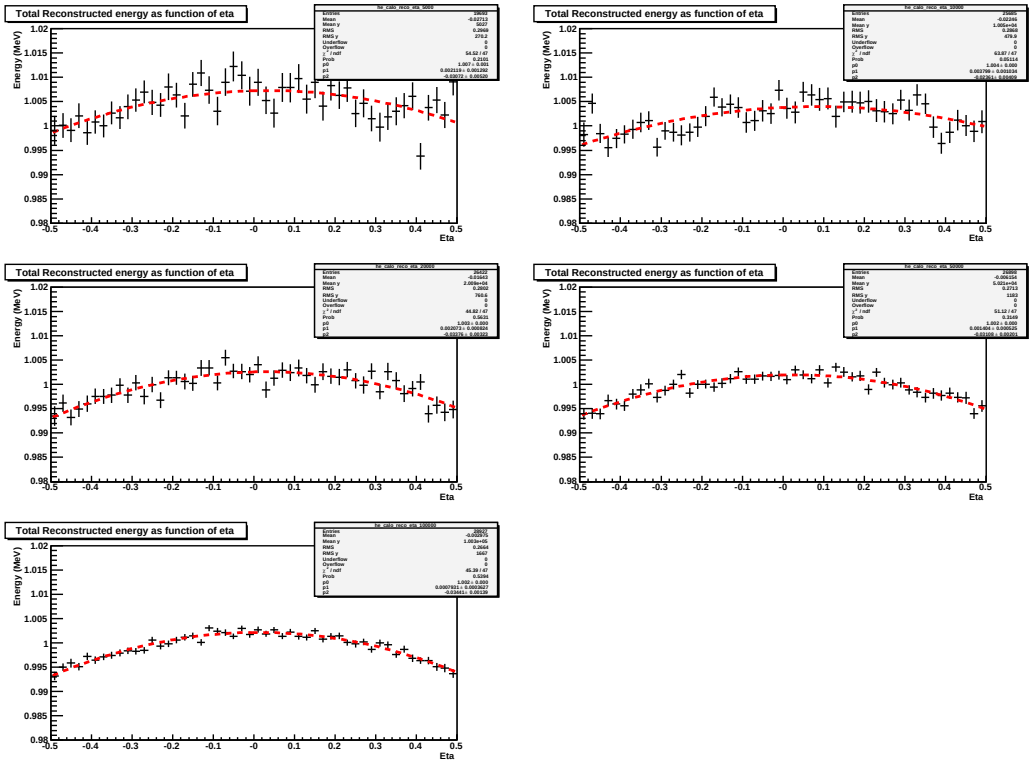

Figure 33: Ratio of the reconstructed energy and the simulated energy as a function of the impact point inside the cell (*energy* h *modulation*) in normalized h cell units at h= 1.2. From left to right and top to bottom 5, 10, 20, 50 and 100 GeV electron energies are shown.

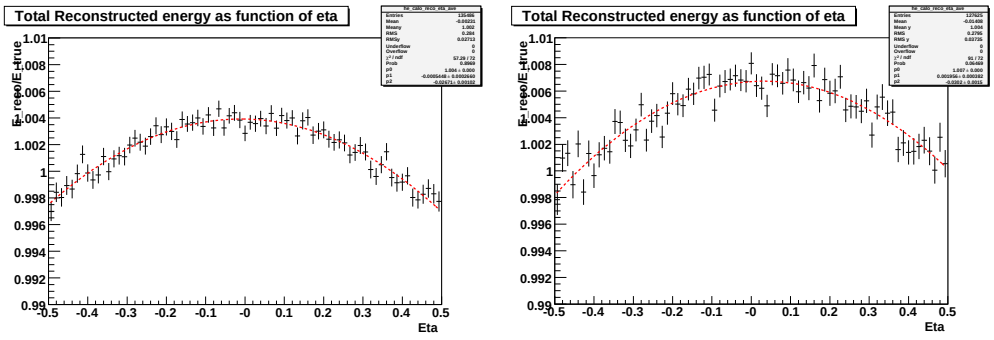

(a) h=0.3 (b) h=1.2

Figure 34: *Energy* h *modulation* averaged on simulated electron energies.

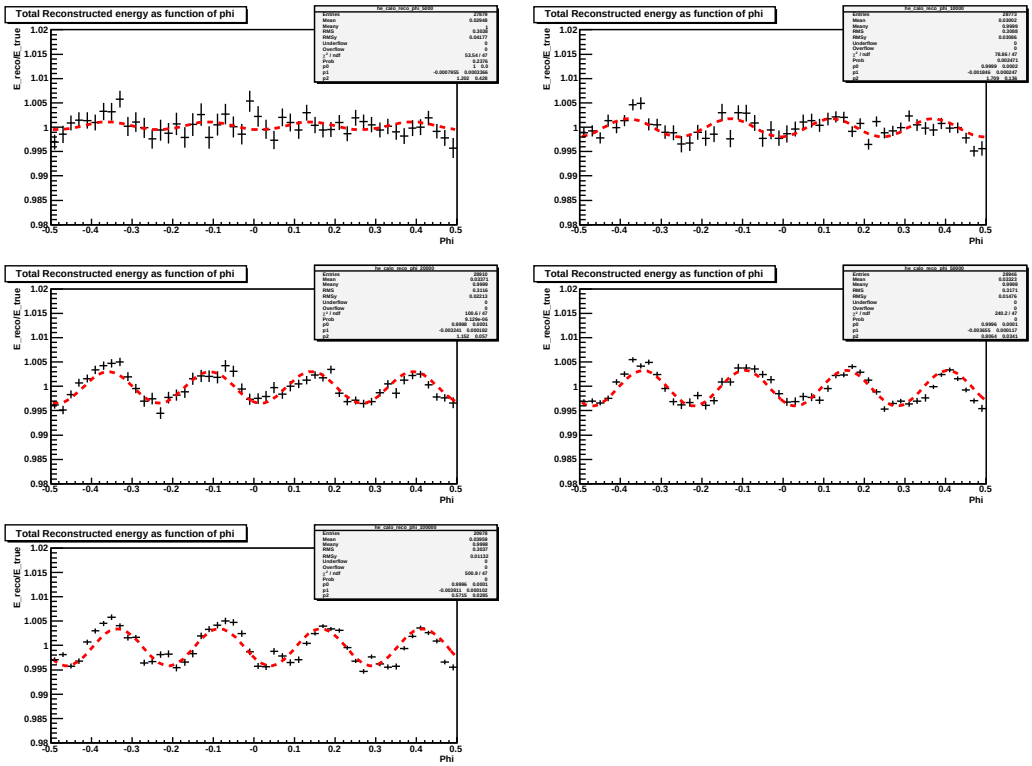

Figure 35: *Energy* f *modulation* for various reconstructed energies at h=0.3. From left to right from top to bottom the electron energies are: 5, 10, 20, 50, 100 GeV. The red dashed line shows the used parametrization.

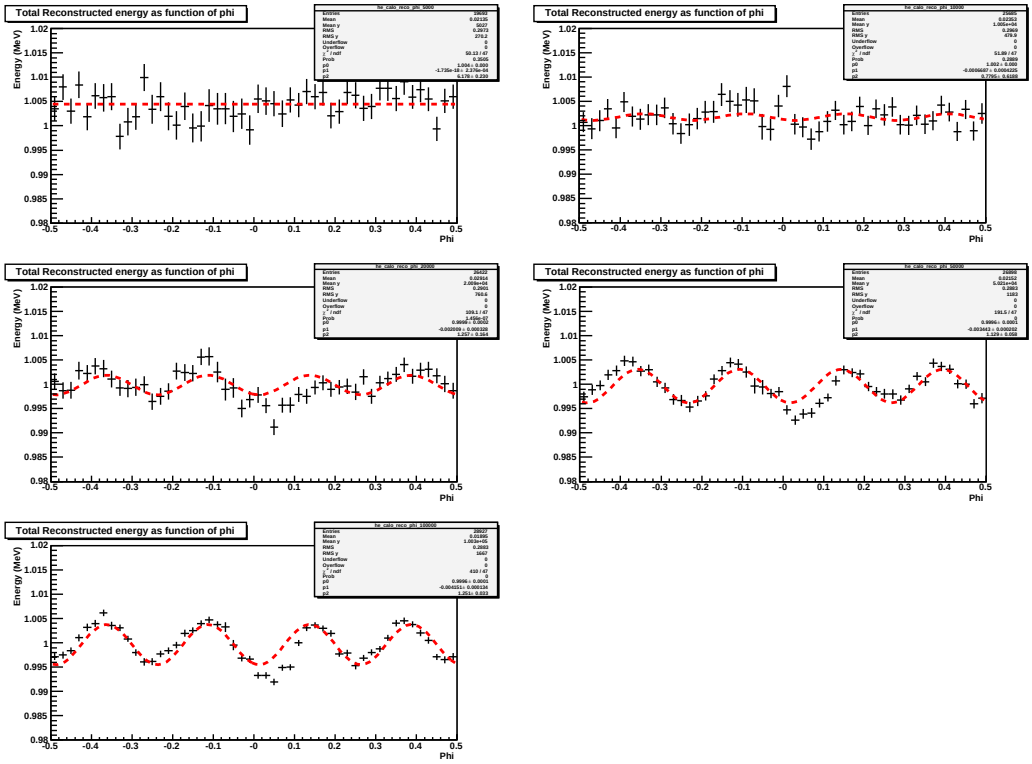

Figure 36: *Energy* f *modulation* for various reconstructed energies at h=1.2. From left to right from top to bottom the electron energies are: 5, 10, 20, 50, 100 GeV. The red dashed line shows the used parametrization.

parametrized as in the equation (14), and the fitted parameters at each energy are listed in table (6) at $\eta = 0.3$.

$$\frac{E_{reco}}{E_{true}} = p_0 + p_1 \cdot \sin(8\pi\phi_{cell} + p_2) \tag{14}$$

$Energy(GeV)$	p_0	p_1	p_2
5GeV	0.9976 $\pm$ 0.3E-03	-1.196E-03 $\pm$ 0.418E-03	3.324 $\pm$ 0.348
10GeV	0.9968 $\pm$ 0.2E-03	-1.218E-03 $\pm$ 0.281E-03	1.161 $\pm$ 0.233
20GeV	0.9993 $\pm$ 0.1E-03	-2.887E-03 $\pm$ 0.2E-03	0.807 $\pm$ 0.0705
50GeV	0.9976 $\pm$ 0.3E-03	-0.45E-03 $\pm$ 0.34E-03	3.324 $\pm$ 0.348
100GeV	0.999 $\pm$ 0.01E-03	0.357E-03 $\pm$ 0.132E-03	3.691 $\pm$ 0.132
Averaged	0.9992 $\pm$ 0.1E-03	-2.489E-03 $\pm$ 0.121E-03	0.589 $\pm$ 0.0496

Table 6: *Energy* ϕ *modulation* parameters for various electron energies. The values of the parameters computed after averaging on the electron energies are listed in the last line.

As in the case of the dependence from η correction factors averaged on the simulated electron energies will be used. As an example in figure (37) the results are shown for $\eta = 0.3$ and $\eta = 1.2$.

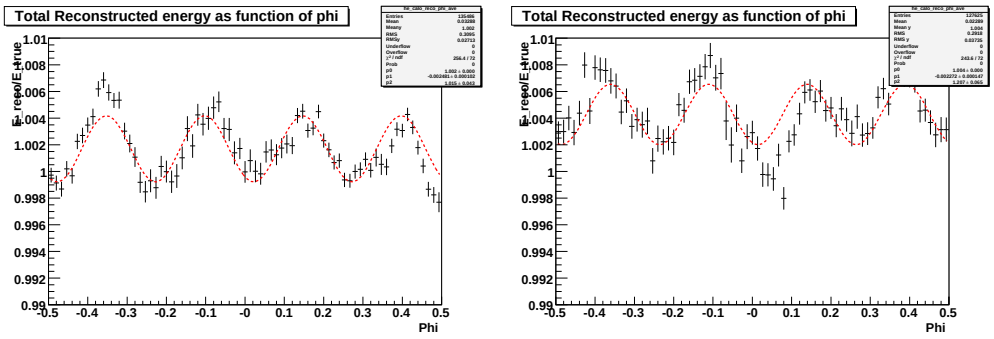

(a) η=0.3 (b) η=1.2

Figure 37: *Energy* ϕ *modulation* averaged on simulated energies. The red dashed line shows the used parametrization.

These corrections are relatively raw. As already said a detailed study of them is outside the aim of this note.

5.4 Resolution and Linearity

The energy resolution and linearity after the impact point dependent corrections are shown in figure (38) and (39).

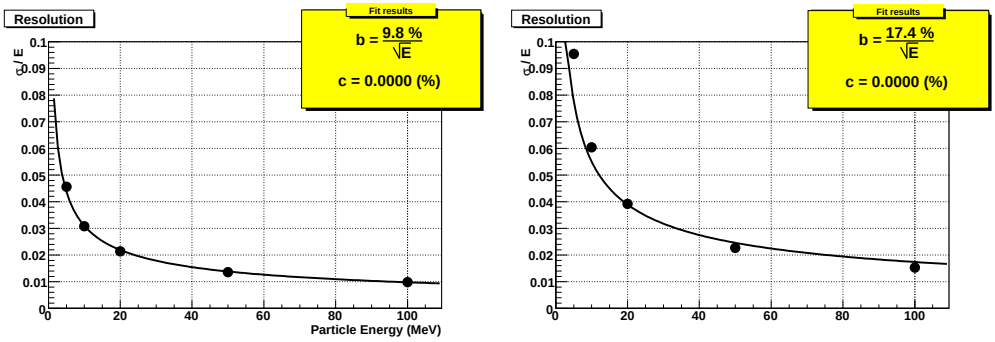

(a) h=0.3 (b) h=1.2

Figure 38: Energy resolution after h and f *energy modulation* corrections

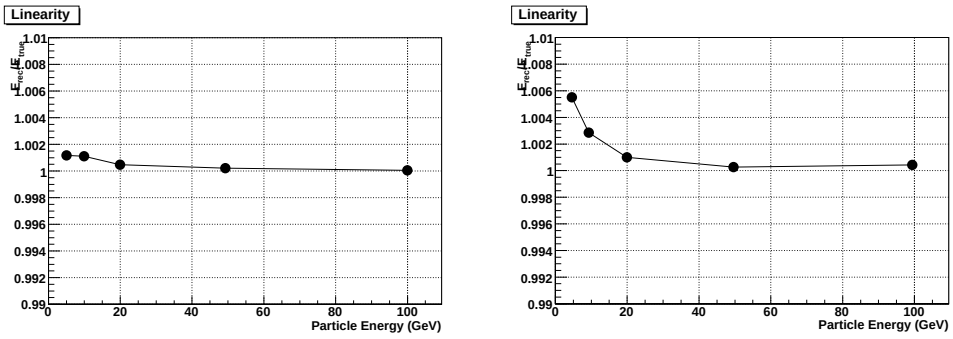

(a) h=0.3 (b) h=1.2

Figure 39: Linearity after h and f *energy modulation* corrections

The sampling term, the constant term and the maximum deviation from the linearity are listed in table (7).

h_{cell}	b(%)	c	Linearity (%)
0.3	9.8	0	0.1
0.6	10.6	0	0.2
0.7	12.0	0	0.3
1.0	14.1	0	0.3
1.1	15.4	0	0.4
1.2	17.4	0	0.5

Table 7: Resolution and linearity after h and f modulation corrections for various h points.

Note that the sampling term of the energy resolution and the linearity are unaffected by the *energy modulation* corrections but, as expected, the constant term is now consistent with zero.

6 Electrons spread over a middle cell and in presence of magnetic field

Last step in our analysis is the study of the effects due to the magnetic field generated by the solenoid. These conditions are the normal operative conditions in ATLAS. It will be shown that the presence of the magnetic field introduces very relevant effects, particularly for low (5-10 GeV) energy electrons:

- Electrons are bent in the ϕ direction
- Photons emitted by bremsstrahlung may hit the calorimeter at some distance from the electron .

Figure (40) shows the correlation between the simulated (true) and the computed ϕ value as discussed in section (5.2) for 5 different energies (from left to right: 100, 50, 20, 10 and 5 GeV). Figure (41) shows the difference between the simulated and the reconstructed ϕ. Note that for 5 GeV electrons the mean deflection is about 0.1 rad i.e. about 4 middle cells. The tails of the distributions are due to events in which the electrons lose a considerable energy in the tracker.

As an extreme example of the effects introduced by the magnetic field, the energy deposited in the calorimeter by a 5 GeV electron (η=0.3, ϕ=0.3) is shown in figure (42). Two clear energy depositions are visible: one due to the electron and one due to a 1.621 GeV photon radiated at a radius of 51.0 mm from the vertex. The use of a fixed dimension cluster algorithm (3X5), as the one used in the present study, underestimates the electron energy by one third. The handling of the electron energy reconstruction when an hard bremsstrahlung occurs is outside the scope of this study. In the following we antiselect events in which a photon of energy greater than 40% of the initial electron energy is radiated. In future a selection based on official electron identification cuts will replace this criteria.

6.1 Reconstruction of the electron impact point

In the Geant4 ATLAS simulation used in the present analysis the impact point of the electron on the calorimeter is not recorded. This prevents a comparison between the impact point coordinates and the barycenter values and the study of the η and ϕ *energy modulation* corrections. As a consequence in the following no impact point dependent corrections were applied.

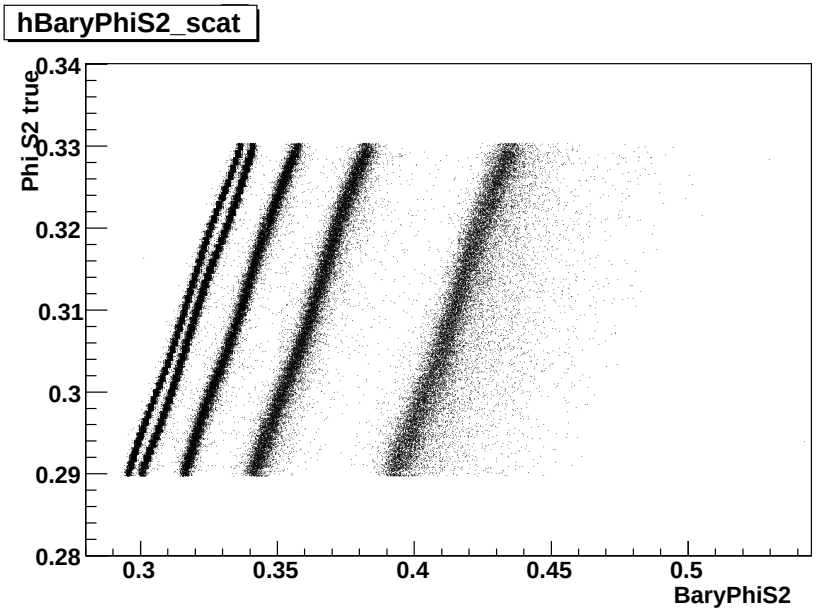

Figure 40: The simulated versus the reconstructed f value for 5 different energies. From left to right: 100, 50, 20, 10 and 5 GeV

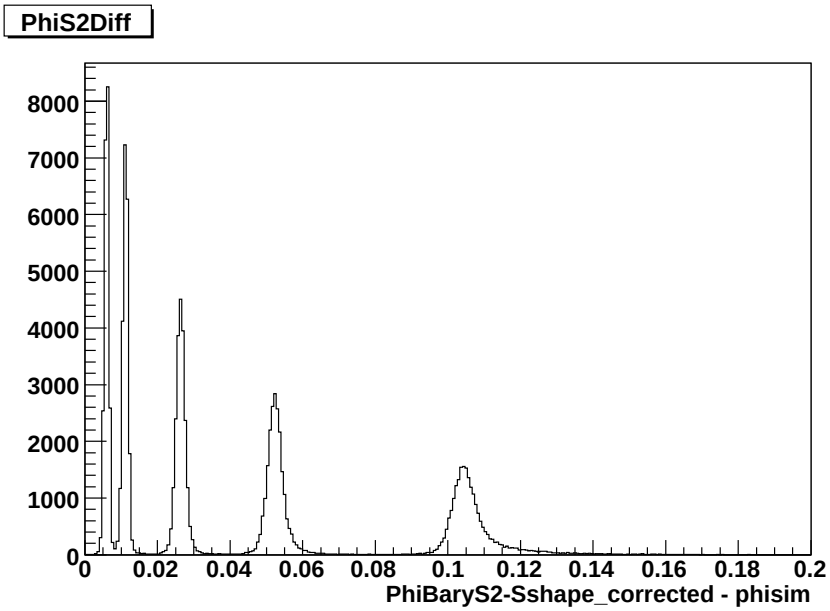

Figure 41: Difference between simulated and reconstructed f value. Peaks correspond to different energies. From left to right: 100, 50, 20, 10, 5 GeV.

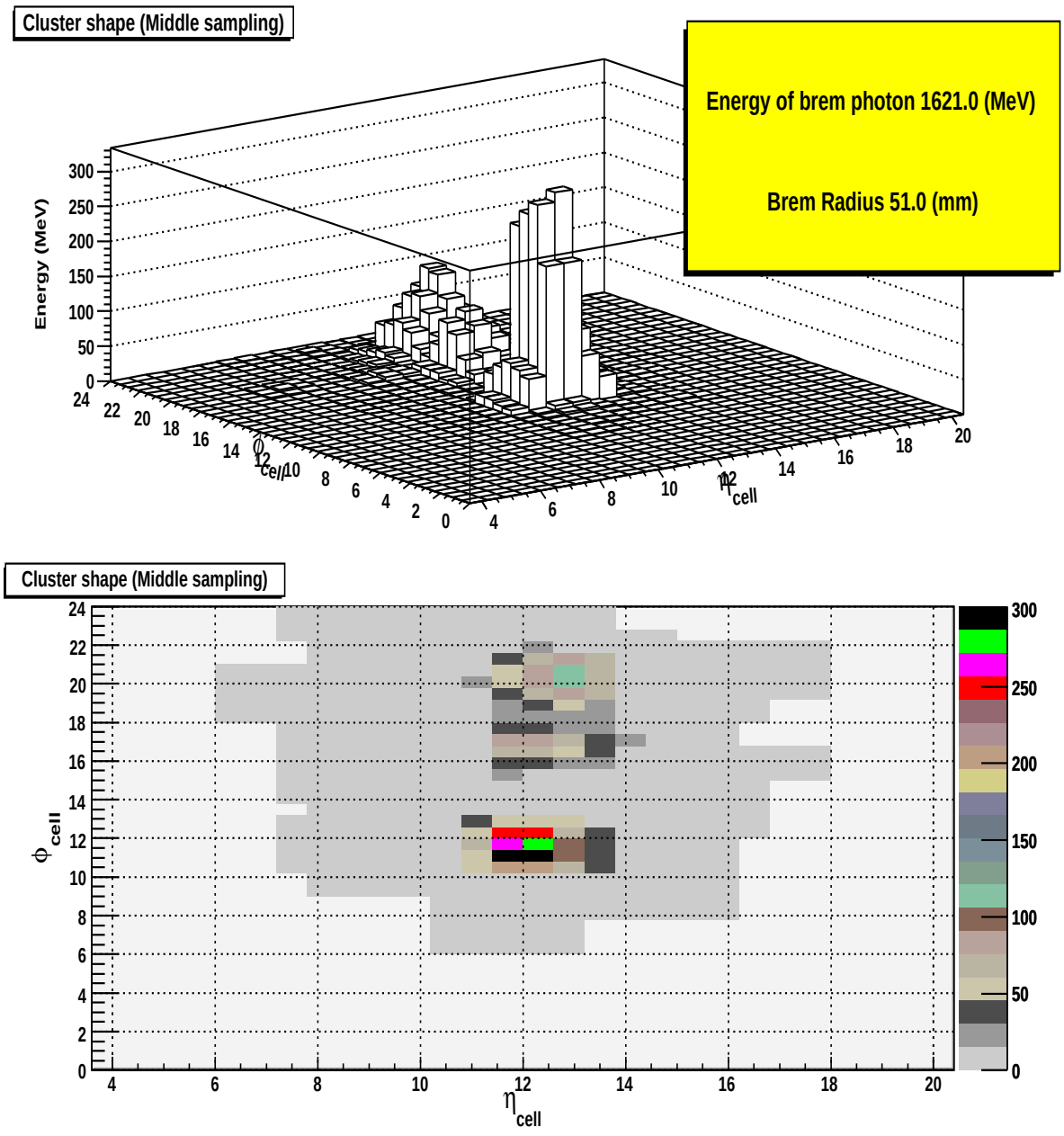

Figure 42: Energy deposited in the calorimeter by a 5 GeV (h=0.3 f=0.3) electron. The electron radiates a photons of 1.621 GeV in the inner detector.

6.2 Computation of the electron energy deposited in the Accordion

In figure (43) the *Total Accordion Correction Factor* (the factor needed to compute the total energy deposited into the Accordion from the energy measured in the cluster) at h=0.3 and h=1.2 is shown as a function of the *shower depth*. Differently from what obtained without magnetic field and shown in figure (8), the correction factor is now strongly energy dependent. While, as shown in figure (44), the sampling fraction in the cluster is still fairly energy independent, the correction for the energy deposited out of the cluster, shown in figure (45), is strongly energy dependent. Low energy electrons deposit up to 50% of their energy outside the cluster. This is due to photons radiated by the electrons and hitting the calorimeter more than three cells from the electron impact point.

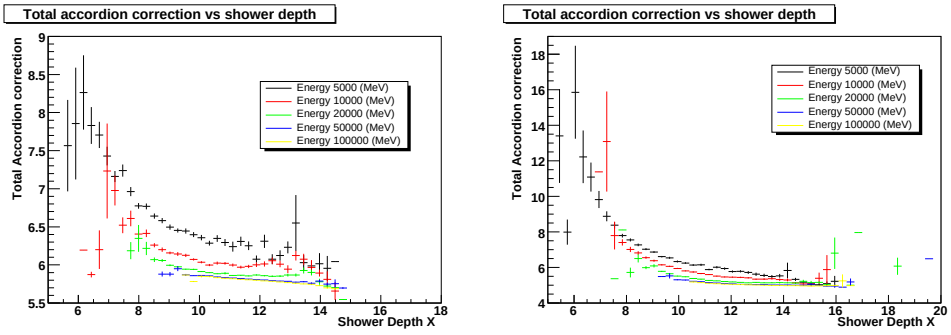

(a) h=0.3 (b) h=1.2

Figure 43: *Total Accordion Correction Factor* when the magnetic field is present.

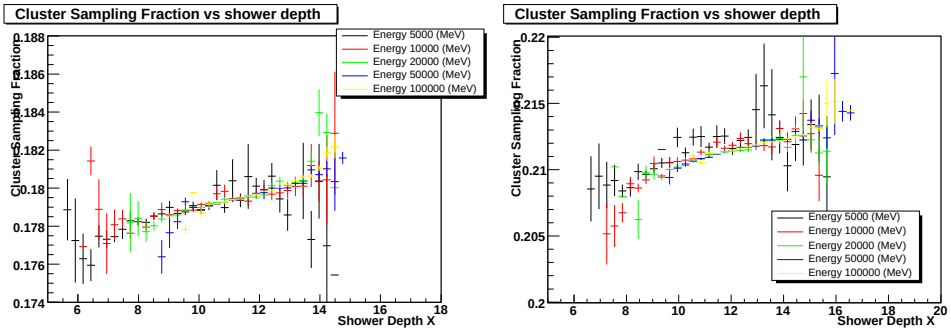

(a) h=0.3 (b) h=1.2

Figure 44: Cluster sampling fraction.

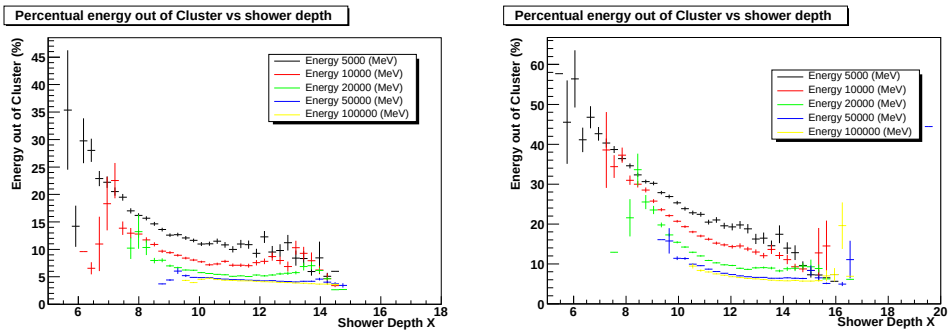

(a) h=0.3 (b) h=1.2

Figure 45: Ratio of the energy deposited outside and inside the cluster.

The energy deposited out of the reconstructed cluster for various shower depth intervals (all electron energies added) are shown in figure (46). The profiles corresponding to low values of the shower depth are more populated by low energy electrons (5 and 10 GeV) and, as expected, show longer tails.

For each electron energy and in each shower depth interval the peak present in the out of cluster energy profile is fitted with a gaussian. Figure (47) shows the gaussian mean values as a function of the shower depth for the various electron energies. The gaussian mean value is energy independent and the fraction of energy outside the cluster is similar to the one computed when the magnetic field is off. This procedure is equivalent to consider only electrons which radiate little energy in the tracker. Finally the fitted out of cluster energy averaged over all energies is linearly parametrized as a function of X and used as correction factor. The result is shown in figure (48). A non linear dependence is visible at high h value. However a higher degree polynomial parametrization does not significantly improve the energy resolution and linearity. A linear parametrization is used in the following.

The inverse of the cluster sampling fraction is also energy independent and it is parametrized as a function of X by a second degree polynomial. The *Total Accordion Correction Factor* is obtained applying in sequence the corrections for the cluster sampling fraction and the energy deposited out of cone.

6.3 Energy deposited in front of the calorimeter

The presence of the magnetic field does not require modifications to the way the energy deposited in the material in front of calorimeter is computed. Figures (49) and (50) show the energy deposited in front of the calorimeter as function of the energy deposited in the preshower for the various electron energies and for h= 0.3

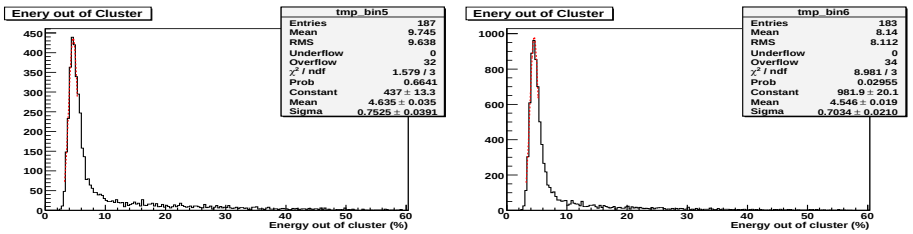

(a) $6 < X \leq 7$

(b) $7 < X \leq 8$

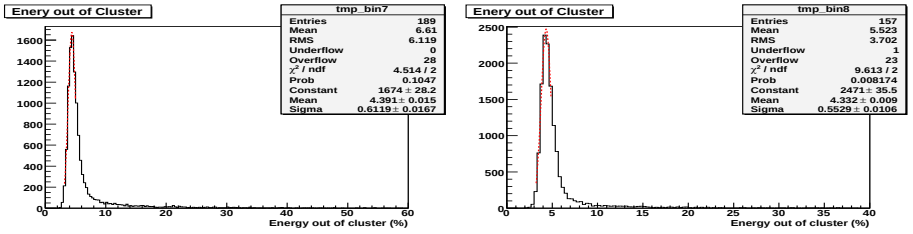

(c) $8 < X \leq 9$

(d) $9 < X \leq 10$

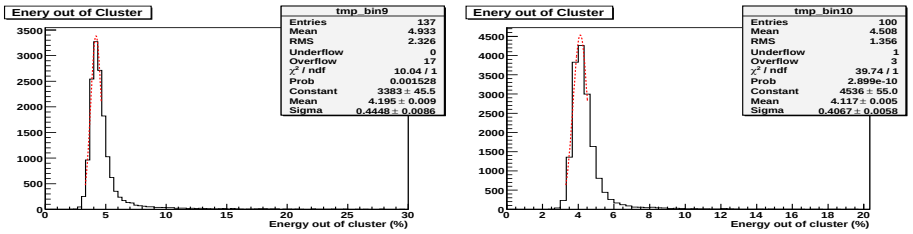

(e) $10 < X \leq 11$

(f) $11 < X \leq 12$

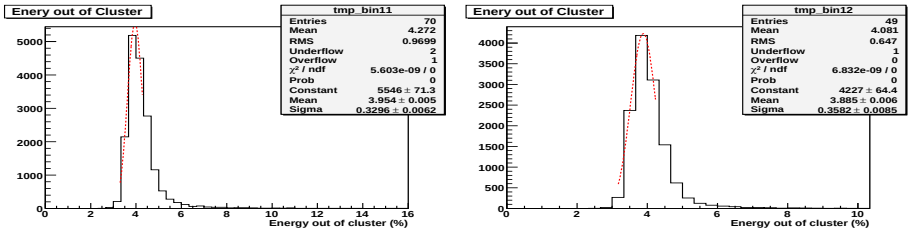

(g) $12 < X \leq 13$

(h) $13 < X \leq 14$

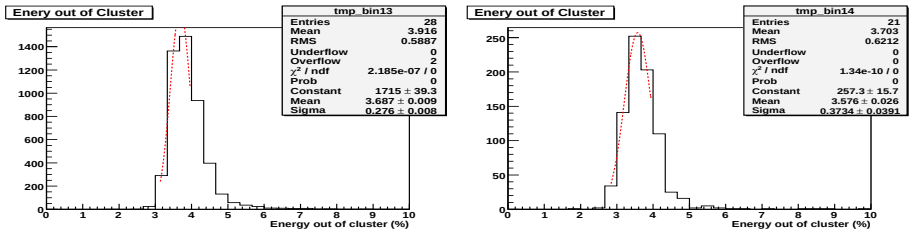

(i) $14 < X \leq 15$

(j) $15 < X \leq 16$

Figure 46: The out of cluster deposited energy (%)for various shower depth intervals (all electron energies added) at h=0.3.

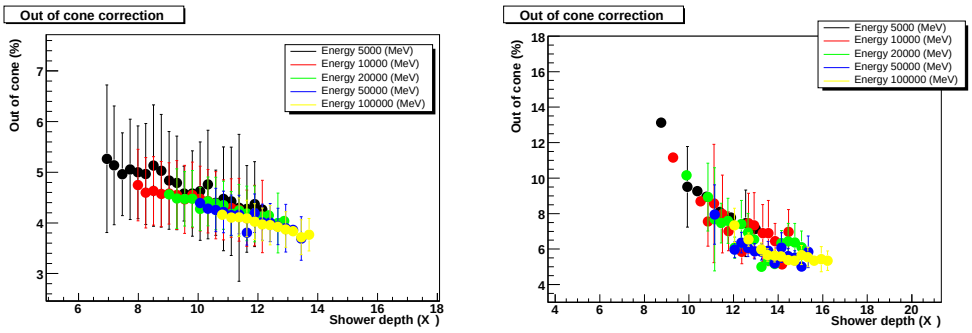

(a) h=0. (b) h=1.2

Figure 47: Fraction of energy out of cluster obtained by the Gaussian fit discussed in the text for various electron energies as a function of X.

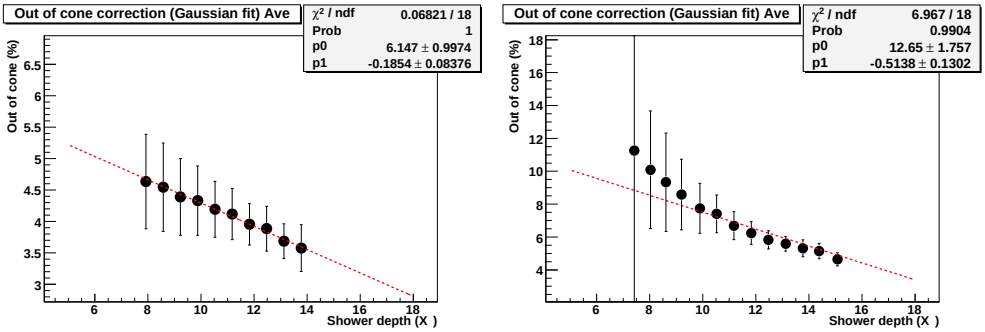

(a) h=0.3 (b) h=1.2

Figure 48: Fraction of energy out of cluster obtained by the Gaussian fit discussed in the text averaged over electron energies as a function of X.

and h=1.2.

The parameters used to compute the deposited energy (*offset and slope*) are shown in figure (51) as a function of the mean energy deposited in the Accordion.

6.4 Longitudinal leakage correction

The correction for the longitudinal leakage is parametrized as in the no magnetic field case. In figure (52) the ratio between the energy deposited behind and inside the Accordion mediated over all energies is shown as a function of the shower depth for h=0.3 (left) and h=1.2 (right).

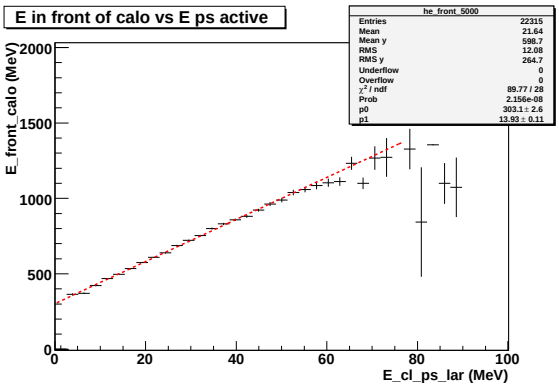

(a) E_e=5GeV

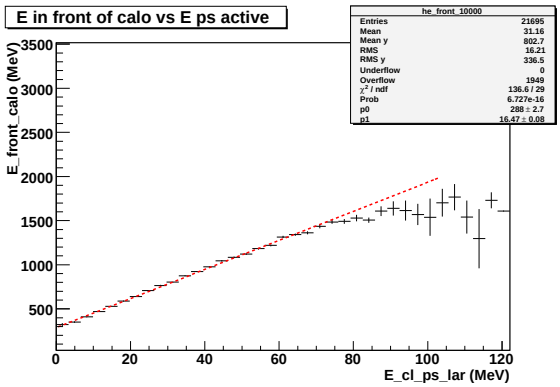

(b) E_e=10GeV

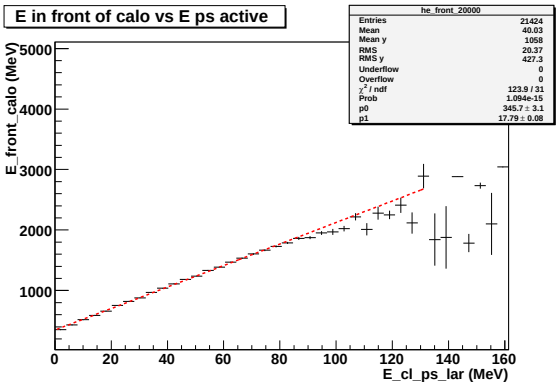

(c) E_e=20GeV

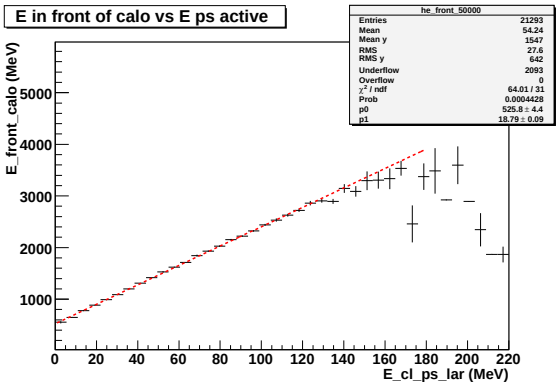

(d) E_e=50GeV

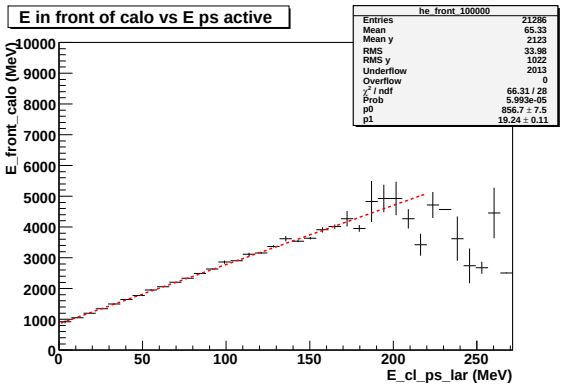

(e) E_e=100GeV

Figure 49: Energy deposited in front of the calorimeter as a function of energy in the preshower at h=0.3 for the various electron energies.

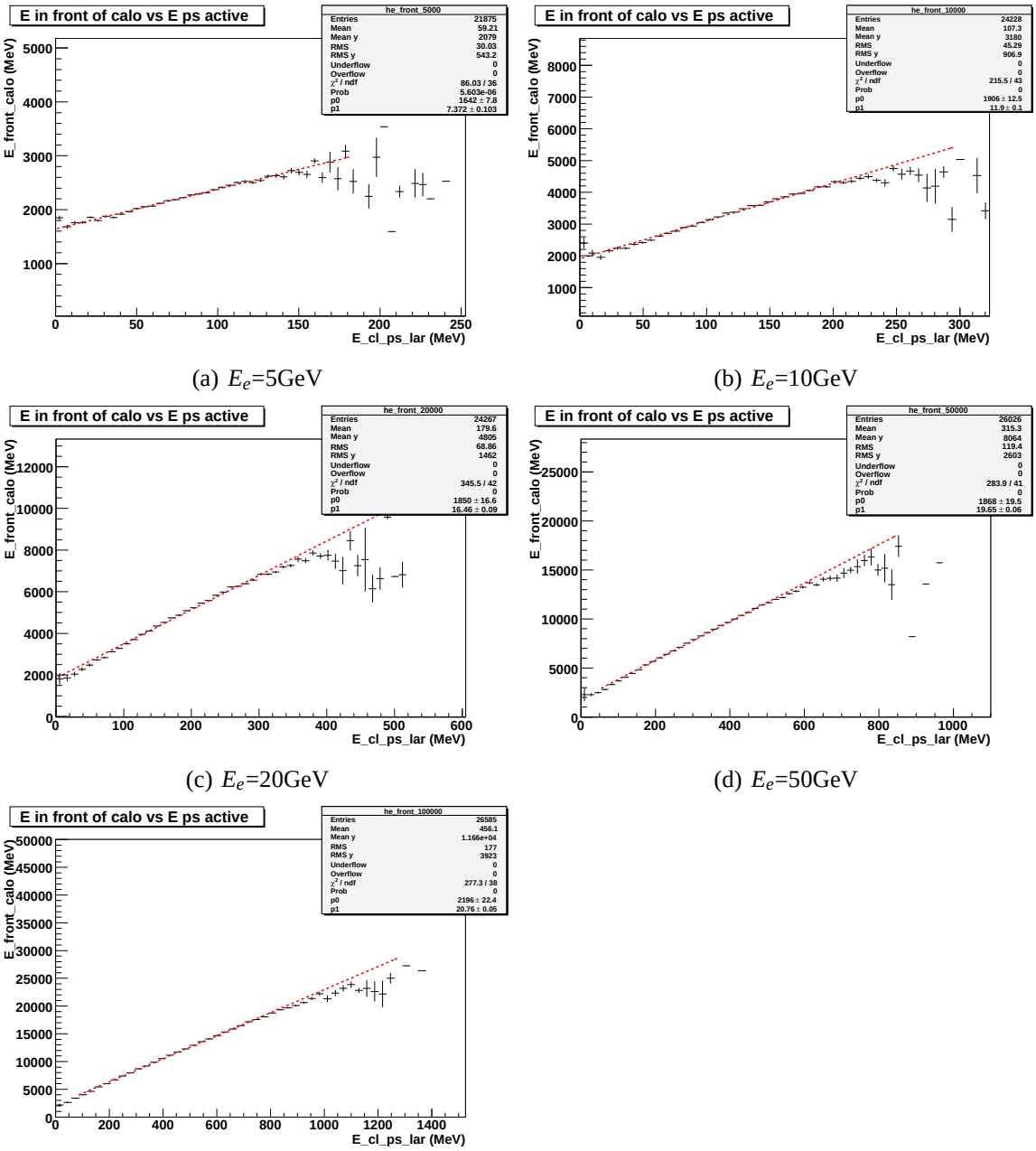

(a) E_e=5GeV

(b) E_e=10GeV

(c) E_e=20GeV

(d) E_e=50GeV

(e) E_e=100GeV

Figure 50: Energy deposited in front of the calorimeter as a function of energy in the preshower at h=1.2 for the various electron energies.

6.5 Resolution and Linearity

The energy profi les for electrons of 5,10, 20,50 and 100 GeV are shown in fi g.(53) and (54) at h = 0.3 and h = 1.2. A gussian fi t in the interval $-2 < s < +2$ gives

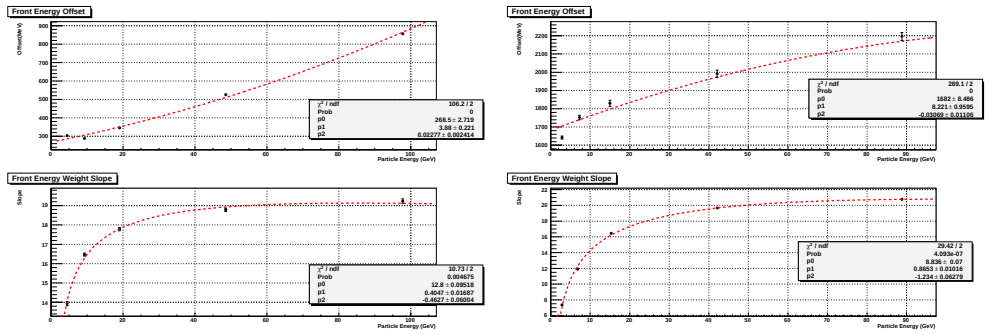

(a) h=0.3 (b) h=1.2

Figure 51: *Offset and slope* as a function of average energy lost in the Accordion. Plots at the top show the offset, the bottom show the slope. Supersimposed are the results of the parametrization

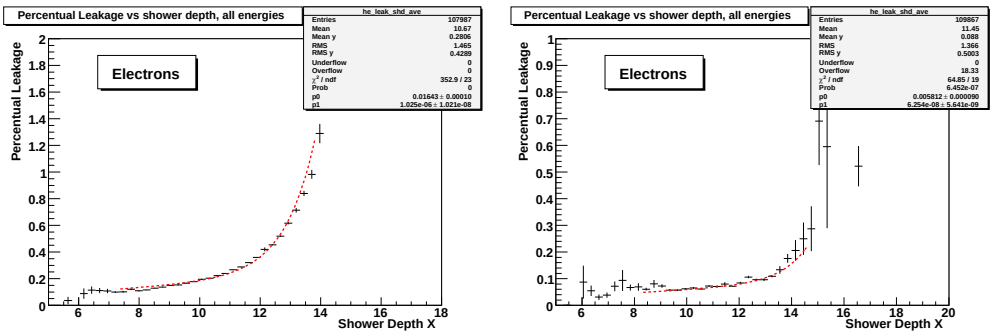

(a) h=0.3 (b) h=1.2

Figure 52: Ratio between the energy deposited behind and inside the Accordion mediated over all energies as a function of the shower depth.

mean value and standard deviation for each sample.

The computed sampling and costant terms of the energy resolution and the maximum values of the *linearity* are listed in table (8) and shown in figure (55) and (56) for h= 0.3 and 1.2 respectively. In the last column of table (8) the maximum values of the linearity is listed when the 5 GeV electrons are not considered. The energy resolution is only marginally affected by the magnetic field as can be seen comparing table (2) and table (8). On the contrary the deviation from the linearity are more severe reaching up to 1.5% at latge h and low energy electrons (5 GeV). This is due to the combined effects of the magnetic field and the significant amount of material in front of the calorimeter.

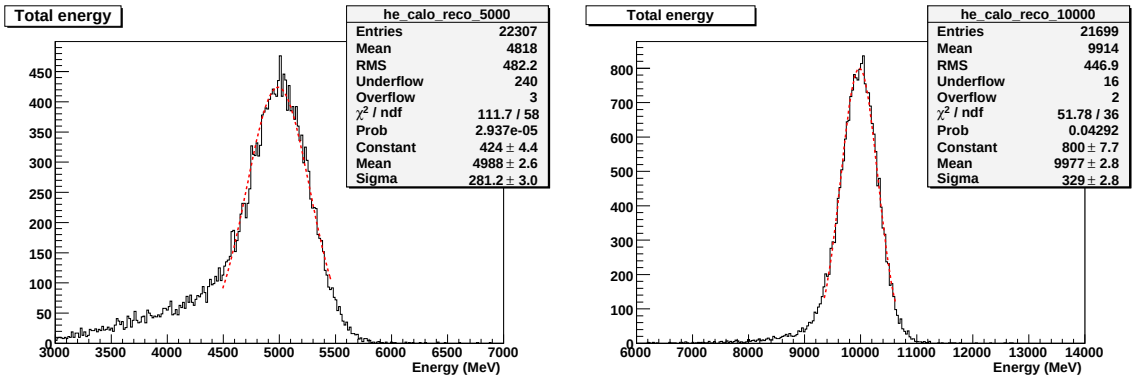

(a) E_e=5GeV

(b) E_e=10GeV

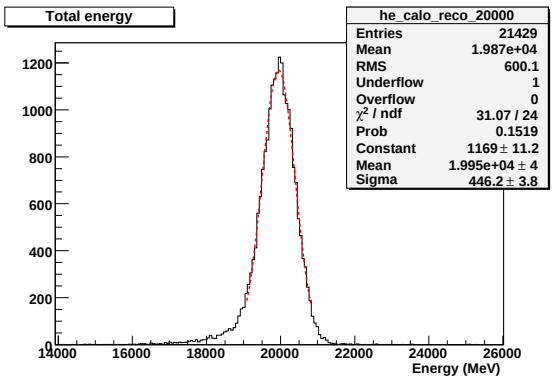

(c) E_e=20GeV

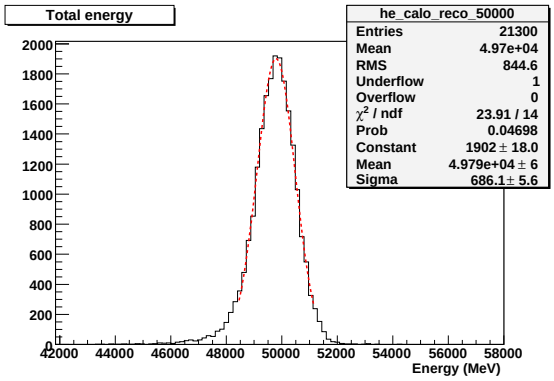

(d) E_e=50GeV

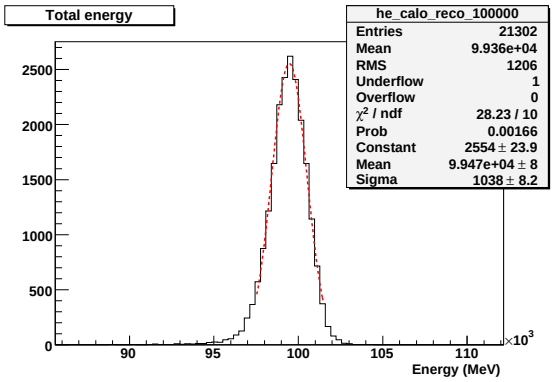

(e) E_e=100GeV

Figure 53: Energy profiles at h=0.3 for the various electron energies.

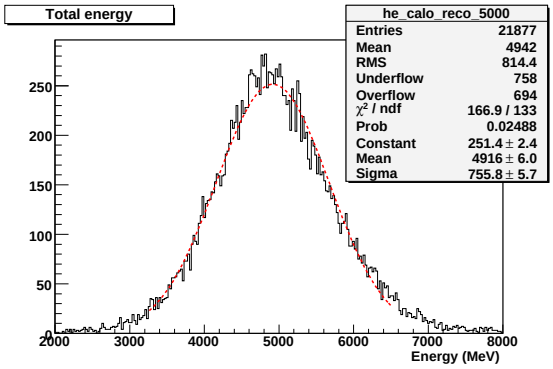

(a) E_e=5GeV

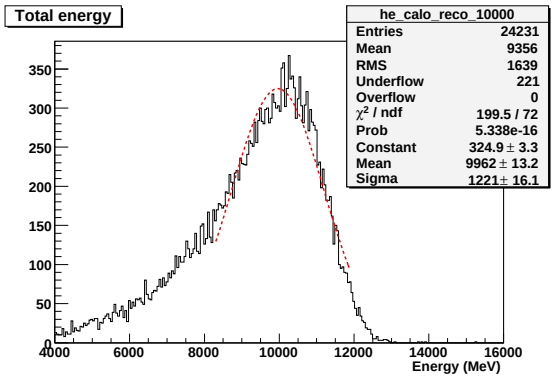

(b) E_e=10GeV

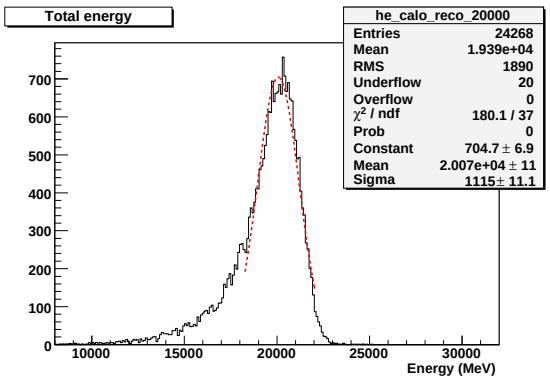

(c) E_e=20GeV

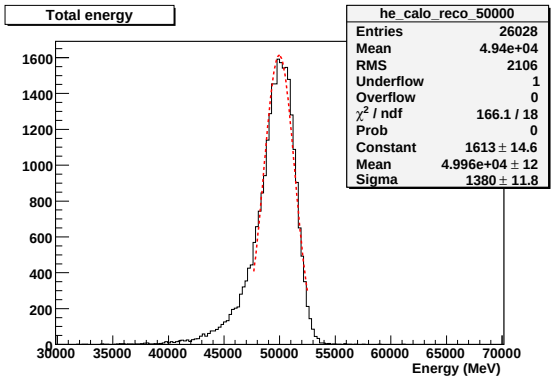

(d) E_e=50GeV

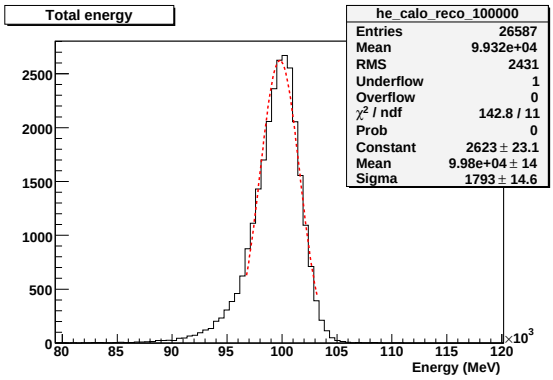

(e) E_e=100GeV

Figure 54: Energy profiles at h=1.2 for the various electron energies.

h_{cell}	$b(\%)$ $(\sqrt{GeV})$	$c(\%)$	Linearity (%)	Linearity $E > 5GeV$ (%)
0.3	9.9	0.274	0.2	0.1
0.6	10.8	0.242	0.3	0.1
0.7	12.2	0.220	0.5	0.2
1.0	13.4	0.275	0.5	0.3
1.1	13.7	0.247	0.6	0.3
1.2	16.8	0.240	1.5	0.4

Table 8: Sampling term, constant term and maximum value of the linearity with the solenoid magnetic field on for various h values. No corrections dependent from the impact point are applied. The linearity values in the last column are for electrons with energy 5 GeV

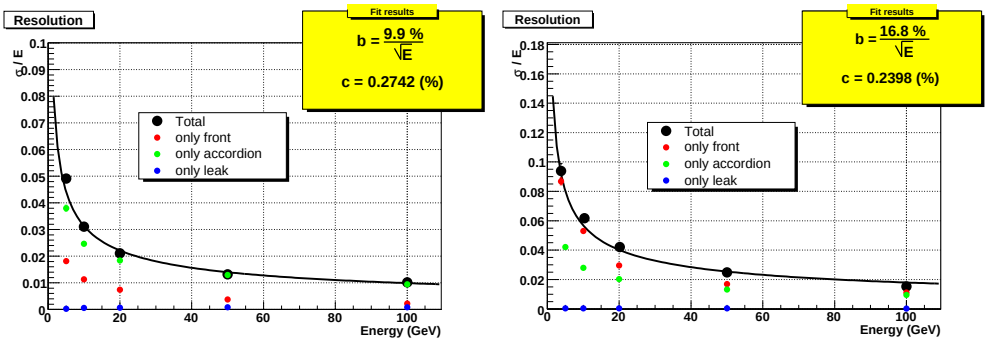

(a) h=0.3 (b) h=1.2

Figure 55: Energy resolution with the solenoid magnetic field on. No corrections dependent from the the impact point are applied.

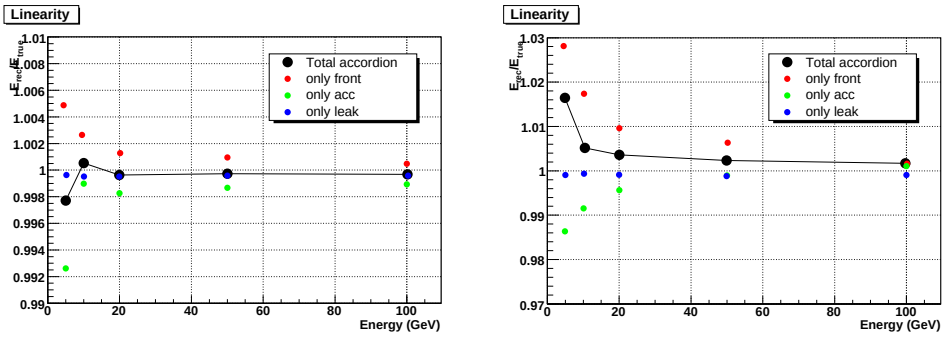

(a) h=0.3 (b) h=1.2

Figure 56: Linearity with the solenoid magnetic field turned on. No corrections dependent from the impact point are applied.

Conclusions

The present note shows how with the technique of the *Calibration Hits* the electron energy can be reconstructed with good energy resolution and excellent linearity in the Barrel Accordion calorimeter. Aiming at the understanding of the various effects contributing to the energy resolution and linearity the study was performed starting from the simplest possible conditions (no magnetic field, electrons at the center of a cell). Finally the nominal ATLAS conditions (magnetic field on and electrons spread uniformly over a middle cell surface) are considered. A peculiarity of the proposed method is that it allows to compute the various contributions to the electron energy reconstruction : energy deposited in front of the Accordion, in the Accordion itself and behind it. The knowledge of these quantities is interesting in itself and could be of great help when operating in ATLAS with the real set up. In normal ATLAS operation conditions the sampling term of the energy resolution varies from 9.9% to 17.8 % for $0.3<|\eta|<1.2$. The maximum deviation from linearity varies from 0.1% and 0.4% in the same pseudorapidity range with the exception of low energy electrons (5GeV) which deviates up to 1.5 %. The electron energy is a function of measured quantities and 11 parameters dependent from the cell pseudorapidity and the cluster size. A statistics of few thousand events is sufficient to compute the coefficients at each η value. Work is going on to extend this technique to photons and to the Accordion End Caps and the plan is to prepare a package to be used in Athena.

Acknowledgments

We are very grateful to the Milan computing team for the support in jobs processing. We are also very grateful to T. Carli who first suggested the present calibration method and to G. Unal for suggestions and support.

References

[1] M.Aharrouche et al. *Energy Linearity and Resolution of the ATLAS Electromagnetic Barrel Calorimeter in an Electron Test-Beam*. *NIM A*, 568:601–623, 2006.

[2] Graziani G. *Linearity of the response to test beam electrons for EM Barrel module P13 . ATLAS Note,* ATL-LARG-2004-001, 2004.

[3] M.Aharrouche et al. *Response uniformity of the ATLAS Liquid Argon calorimeter . submitted to NIM*.

[4] LAr ATLAS Collaboration. *Liquid Argon Calorimeter-Technical Design Report*. CERN LHCC 96-41.

All ATLAS internal notes approved by the Collaboration are accessible through the web at http://cdsweb.cern.ch/ *by typing the document identifier (e.g.* ATL-LARG-****) in the search field.*